

54. Organic Materials for Chemical Sensing

Organic Mate

Organic materials for chemical sensing are broadly classified into three categories: (i) macrocyclic compounds, (ii) conducting polymers and (iii) cavitand molecules. A short review of current progress in semiconductor oxide sensing materials is given, pointing out their strengths and limitations. Principal wet techniques for depositing organic thin films are described and electrical, optical and structural properties of all three types of organic materials are analysed in relation to their importance in chemical sensing. Examples of recent advances in chemical sensing of different analytes and pollutants are presented.

54.1	Analyte Requirements	1242	54.3.1	Preparation of Sensing Membranes	1245
54.2	Brief Review of Inorganic Materials	1243	54.3.2	Thin-Film Properties	1248
54.3	Macrocyclic Compounds for Sensing	1245	54.4	Sensing with Phthalocyanine and Porphyrin	1250
			54.4.1	Amperometric Sensor	1250
			54.4.2	Optical Sensors	1251
			54.4.3	Detection of Volatile Organic Vapour Compounds	1254
			54.5	Polymeric Materials	1255
			54.5.1	Conducting Polymers	1255
			54.5.2	Ion Sensing	1257
			54.5.3	Examples of Other Polymeric Sensors	1257
			54.6	Cavitand Molecules	1259
			54.7	Concluding Remarks	1261
			References		1262

The development of a new generation of sensors involves the study of fine-tuned sensor-active materials and transducers [54.1, 2]. Metal oxides, polymer/polymer composites, and dyes are being regarded as key sensing materials. This chapter is organised into eight sections. The next section presents a summary of the needs for chemical sensing of different pollutants. The second section provides a brief description of different semiconducting oxide materials and their applications in sensor technology. Organised ultrathin organic films of molecular and polymeric semiconductors are currently the focus of considerable research with an emphasis on a molecular understanding of the sensing mechanisms. The low cost of fabrication, large-area processability, and widely diverse and tailorable physical, electronic, and optical properties have stimulated interest in their practical exploitation. Phthalocyanine and the related macrocyclic compounds have been extensively investigated for chemical sensing primarily because the desired functionality of phthalocyanine molecules can be achieved by changing the central metal atom or introducing substituents in their π -electron aromatic ring [54.3]. The third section is devoted to thin-film formulation of these

interesting compounds and their structural, electrical and optical properties relevant to sensing different types of pollutants. Important transduction methods and their applications in the development of practical sensors are presented in the fourth section, with an emphasis on the interaction at the interface of analyte/film of macrocyclic compounds. The ability of conducting polymers to change their physical properties during reaction with various redox agents makes them very useful for the development of gas sensors. The most common are polyaniline (PAni) and polypyrrole (PPY). It has been shown that the resistivity of polypyrrole increases in the presence of a reducing gas such as ammonia, but decreases in the presence of an oxidising gas such as nitrogen dioxide. The gases cause a change in the near-surface charge-carrier density by reacting with surface-adsorbed oxygen ions [54.4]. Sensing properties of polymers and their importance in the development of intelligent sensors are described in Sect. 54.5. A class of supramolecules, called cavitands, that exhibit discotic phases depending on the structure, are shown to have potential for sensing applications [54.5]. Section 54.6 deals with the applications of thin films of these

molecules such as calixresorcinarene for recognition of organic vapours. The chapter concludes by highlighting

the trends of future development of sensor materials and technology in Sect. 54.7.

54.1 Analyte Requirements

The detection of pollutant gases and volatile organic compounds (VOC) whether in gaseous phase or dissolved in water is of great environmental importance due to the extreme hazards posed by their presence in small amounts in the ambient. Nitrogen dioxide (NO₂), ozone (O₃), sulphur dioxide (SO₂), particulate matter (PM), carbon monoxide (CO), and lead (Pb) are six principal pollutants of major concern for maintaining the quality of air in urban areas (Table 54.1). Some of these pollutants, like CO, Pb, NO₂, PM and SO₂, are emitted directly from a variety of sources including industrial production growth and increased traffic congestion. Ozone is generally formed when emissions of NO₂, SO₂, ammonia (NH₃), VOCs, and other gases react in the atmosphere. The presence of ozone in high concentration is also possible in offices where laser printers and photocopiers are heavily used. On the other hand, water is commonly treated with O₃ to destroy microbial contaminants such as *Escherichia coli* and salmonella [54.6, 7] and there is a need for accurate calibration of ozone content. Due to its ability in absorbing ultraviolet (UV) radiation from sunlight, stratospheric ozone filters out damaging ultraviolet radiation from the sun. Monitoring of ozone in the stratosphere has thus become a global issue as it forms a protective shield for all forms of life on Earth.

Stringent domestic and international standard for emission control requires the monitoring of threshold

limit value of these pollutants in order to protect primarily against adverse public health hazards. For example VOCs and nitric oxide (NO_x) resulting from combustion processes cause respiratory problems. Benzene itself is regarded as a human carcinogen and vehicle exhaust is primarily composed of these toxic gases. Spillage in fuel stations also contribute to the emission of excessive amounts of aromatic hydrocarbons in the atmosphere. VOCs also bind with ground-level ozone and form a photochemical smog, causing breathing difficulty for asthma sufferers. The secondary requirement of pollution monitoring is to reduce disastrous effects on the preservation of ecosystems, plants and animals. Safeguard is also to be taken against the decreased visibility due to the presence of PM and damage to crops, vegetation, and buildings due to atmospheric pollution. The SO₂ content is known to attack the indoors and outdoors of buildings, and in particular the surface of historical glasses. A wide variety of preventive conservation tools and routines have been sought to protect historical and cultural objects against deterioration and degradation [54.8, 9].

The activities of chemical sensing are not solely limited to environmental control. Hydrogen (H₂) fuel cells are clean, quiet, more efficient generators of electricity than any other known technology. Hydrogen is also an important raw material for the aerospace, chemical and semiconductor industries. As hydrogen is explosive above the lower explosive limit (LEL), H₂ sensors have

Table 54.1 Air quality standards for the UK, USA and World Health Organisation (WHO)

Pollutant	UK		WHO		USA	
	Concentration	Standard measured	Concentration	Standard measured	Concentration	Standard measured
Benzene	5 ppb	Annual mean	Data not available			
1,3-butadiene	1 ppb	Annual mean	Data not available			
Carbon monoxide (CO)	8.6 ppm	8 h mean	8.6 ppm	8 h mean	9 ppm	8 h mean
Lead (Pb)	0.25 µg/m ³	Annual mean	0.5 µg/m ³	Annual mean	1.5 µg/m ³	Quarterly mean
Nitrogen dioxide (NO ₂)	21 ppb	Annual mean	105 ppb	1 h mean	0.05 ppm	Annual mean
Ozone (O ₃)	50 ppb	8 h mean	60 ppb	8 h mean	0.08 ppm	8 h mean
Particles (PM ₁₀)	50 µg/m ³	24 h mean	70 µg/m ³	24 h mean	50 µg/m ³	Annual mean
Sulphur dioxide (SO ₂)	100 ppb	15 min mean	188 ppb	10 min mean	0.14 ppm	24 h mean

now become important safety devices in all these applications. The oxygen sensor which detects the air–fuel mixture of a gasoline engine by measuring the amount of oxygen in the exhaust gas is an essential component of the car engine management system. The development of reliable oxygen sensors for medical application has received considerable research attention in recent years [54.10–12]. Drinking, industrial and swimming-pool water must be disinfected with suitable oxidising agents such as chlorine or chlorine compounds. The dosing of the appropriate oxidising agents must be carefully controlled to suit the application as a higher concentration can result in corrosion effects, impairment of taste or skin irritation. The ability of detection of chlorine in sub-ppm level is therefore essential [54.13]. Ammonia is increasingly used as a refrigerant alternative to ozone-depleting chlorofluorocarbon (CFC). Large quantities of ammonia can also be found in fertiliser factories, resin production plants using urea, explosives munitions plants, semiconductor industries and water utility facilities. The presence of ammonia can cause inhalation problem at a very low concentration (0.6–53 ppm). Airborne ammonia gas dissolves in moisture on the skin, forming corrosive ammonium hydroxide. The exposure of ammonia at 10 000 ppm is mildly irritating to moist skin but the effects become more pronounced with the increasing concentration, producing chemical burns with blistering at 30 000 ppm. Its solubility in water can cause it to cauterise respiratory tracts, resulting in deaths at concentrations of 5000 ppm. Research into the development of reliable ammonia sensors with

a fast response to a wide range of concentrations is intensive [54.14–16].

It is obvious from the brief survey above that growing demand exists for the fabrication of low-cost, low-power, robust and portable chemical sensors for a variety of pollutants, contaminants and analytes, showing improved sensitivity and selectivity for industrial, healthcare and environmental control. Analytical chemical tools provide advanced and reliable methods for detection of different analytes but those methods are in many cases prohibitively expensive, unsuited for large-scale field measurements or mobile monitoring. For instance, there is currently a good market for detection systems for ozone at low concentration (ppb level) to replace more expensive techniques such as UV absorption measurements [54.17]. Existing devices for the detection of ozone are now mostly based on electrochemical measurements [54.18], or on solid-state semiconductor devices [54.19]. Similarly, the detection of organic vapours involves extracting air samples and subsequently analysing them using standard laboratory techniques such as gas chromatography [54.20], mass spectroscopy and Fourier-transform infrared (FTIR) spectroscopy [54.21, 22]. The major disadvantages associated with these techniques are their complexity, the capital cost of the instruments used and the requirement for trained human resources for operation and the interpretation of data. Apart from environmental applications, the development of detection instrumentation of these species is also important for both human health monitoring [54.23, 24] and for odour detection [54.25].

54.2 Brief Review of Inorganic Materials

Solid-state semiconductor gas sensors are usually made of tin oxide (SnO_2) in the form of thick films, porous pellets or thin-film coatings to monitor the presence of various gases [54.26]. These sensors are being used in the intelligent automatic control of a large number of processes, ranging from microwave cooking to the efficient combustion of motor engines. SnO_2 sensors operate at high temperatures of 300–400 °C. Gases are adsorbed onto the surface in the presence of air and the semiconductor of the metal oxide changes due to the formation of a surface depletion layer. The thickness of this layer can be expressed in terms of the Debye length $L_D = \sqrt{\varepsilon_0 \varepsilon k_B T / (q^2 n_0)}$, where ε_0 is the permittivity of free space, ε is the dielectric constant of the semiconducting material, n_0 is the total carrier concentration, q is the electronic charge, k_B is the Boltzmann constant,

and T is the absolute temperature [54.27]. The sensitivity of the sensor is generally defined as the ratio of the change in the conductance after the treatment to the conductance of the sensor in air and can simply written as $\Delta n L_D / n_0$, where Δn is the change in carrier concentration due to the analyte exposure. It is therefore possible to optimise the sensitivity by reducing grain size, lowering the carrier concentration and increasing the Debye length. The maximum sensitivity is assumed to have been achieved when the Debye length is about half the particle size.

Figure 54.1 shows a photograph of a comb-like interdigitated electrode (IDE) system used for most conductivity measurements. The original idea was developed by *Taguchi* [54.28] and the sample resistance in this configuration is smaller than that obtained from

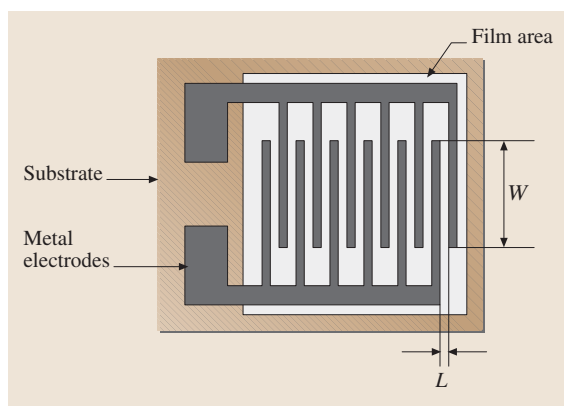


Fig. 54.1 Interdigitated electrode (IDE) system for an SnO₂ sensor

the four-contact geometry. The output signal is normally logarithmic to gas concentration. The conductivity change of SnO₂ thick-film sensors was monitored on exposure to compounds forming in smouldering and combustion processes of natural materials, e.g. paper and wood. A strong response was observed for compounds with hydroxyl groups and the highest response was obtained for phenolic structures such as methoxyphenols and benzenediols [54.29]. The response of a SnO₂ sensor element operating at 270 °C produced no sensor response to toluene, furfural and acetone [54.30]. The impedance output from the SnO₂ sensor array was measured at 300 °C in terms of conductance changes and peak frequency changes. These changes were more the more sensitive to oxygenated VOCs than other VOCs. The sensors sensitivity could also be enhanced by Pd- and Pt-doped sensors [54.31].

Considerable development work is being carried out to integrate the semiconductor sensing membrane with the interrogation and control circuitry on a silicon chip using conventional silicon technology. Using an industrial 0.8- μm complementary metal-oxide-semiconductor (CMOS) process with subsequent micromachining steps, a CO gas-sensor chip was fully integrated with advanced analogue and digital circuitry on a chip for temperature control in the range 170–300 °C with an error of ± 2 °C. The whole device was encapsulated using standard microelectronic packaging methods. It was reported that the integrated sensor was capable of measuring CO at the concentration of 5 ppm with a resolution of ± 0.1 ppm [54.32].

Solid-state sensor technology relies on the preparation of semiconductor films. SnO₂ sensors suffer from a lack of selectivity and drift. The high temperature re-

quired for the surface reactions encourages the growth of grains by coalescence, giving rise to unstable materials. Recent progress in the synthesis of nanomaterials has been employed to overcome some of these problems. Oxide powders were thermally evaporated under controlled conditions without the presence of a catalyst to deposit single-crystalline SnO₂ nanobelts on a platinum IDE structure on an alumina substrate. The surface-to-volume ratio was very high but the size was large enough to contain the depletion layer within the belt. SnO₂ nanobelts were sensitive to CO, NO₂ and ethanol and therefore suitable for applications in breath analysis and food control [54.33].

Advanced methods of information technology are increasingly being used to address the issues regarding selectivity and specificity. A sensor array of two commercial metal-oxide gas sensors was developed to discriminate six organic solvents over a wide concentration range of 2–200 ppm in air. The baseline drift was considerably reduced over a test period of several months by temperature cycling. Further reduction in drift was achieved by suppressing the influence of humidity via additional signal preprocessing. Relatively low computing power was required for the hierarchical pattern classification to evaluate shape features generated from the sensor response curve during temperature cycling. The technique was found to be adaptable to different operating environments, for example, to suppress false alarms from interfering gases [54.34].

Apart from SnO₂, titania (TiO₂), ferric oxide (Fe₂O₃), titania doped chromium oxide (Cr_{1.8}Ti_{0.2}O₃), molybdenum trioxide (MoO₃), tungsten oxide (WO₃), indium oxide (In₂O₃) and perovskite-type thick films (LaFeO₃) were studied for sensing a host of analytes such as H₂, CO, NO₂, H₂S, NH₃ and CH₄ in the ppb range. The characteristics of titanium dioxide nanotube hydrogen sensors were found to be completely reversible, highly selective and free from hysteresis. The sensors showed response times of approximately 150 s at a nominal operating temperature of 180 °C. The sensitivity of the nanotubes was believed to be due to chemisorption of hydrogen onto the titania surface as electron donors. Increased operating temperature improved the sensitivity significantly but reduced the response time. Samples with smaller pore diameter (46 nm) were more sensitive to hydrogen than those with larger pore diameter (76 nm). The sensor showed response to high concentrations of oxygen but the response time was long and the recovery was not complete [54.35]. Ion-beam-deposited thin films of MoO₃ on alumina substrates with gold IDEs showed selective

response to NH_3 at 450°C . Similarly prepared WO_3 thin-film samples were highly sensitive to NO_2 . Both films exhibited orthorhombic structure but the poly-

morphic dissimilarities between two types of materials were responsible for the difference in their sensing behaviour [54.36].

54.3 Macrocylic Compounds for Sensing

Phthalocyanine (**Pc**) molecules belong to a class of macrocyclic compounds. Because of their 18 π -electron aromatic macrocyclic structure these molecules exhibit important optoelectronic, photophysical, conducting and photoconducting properties [54.37]. As shown in Fig. 54.2, the **Pc** structure is closely related to the naturally occurring porphyrins, which form a core skeleton in the haemoglobin and chlorophyll. Organic molecular nanostructures have huge potential but suffer from unstable device characteristics, low resistance to adverse environments (e.g., temperature, humidity, oxygen, etc.) and lack of reproducibility of material composition, purity, and fabrication conditions. **Pcs** are, however, tinctorially strong, chemically and thermally stable. The materials are abundantly available in a highly purified form.

54.3.1 Preparation of Sensing Membranes

Sensing is essentially an interaction mechanism of a solid surface and analytes and the molecules are organised in ultrathin films, offering a large surface-to-volume ratio to improve the probability of these reactions taking place. A variety of methods such as direct-current **DC** and radio-frequency **RF** sputtering [54.38], thermal evaporation [54.39], Langmuir–Blodgett (**LB**) [54.40], spin coating [54.41] and self-assembly (**SA**) [54.42] are employed to produce organised thin organic films.

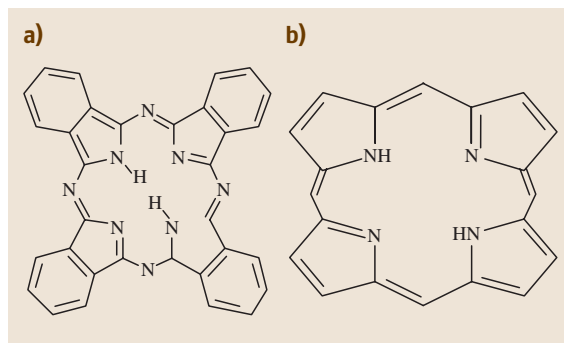


Fig. 54.2a,b Chemical structure of: (a) a metal-free phthalocyanine and (b) porphyrin molecule

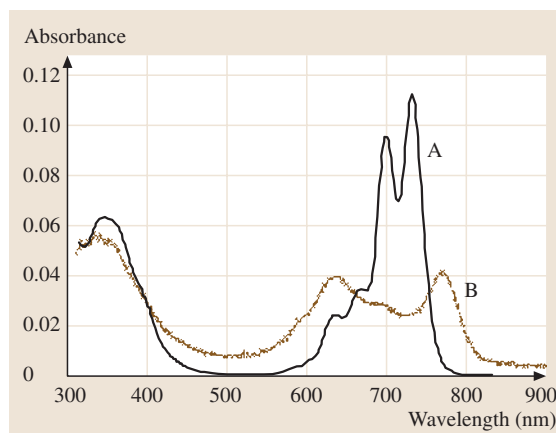


Fig. 54.3 Typical UV–visible spectra for thin films of metal-free phthalocyanine molecules in: (A) chloroform and (B) an **LB** film

The substrates play a key role in determining the film quality and the structure. It is found that the island density and coverage ratio of copper tetra-*tert*-butyl phthalocyanine (**CuTTBPC**) on hydrophilic glass surfaces were small during the early growth stage of vacuum deposition due to a small nucleation rate arising from

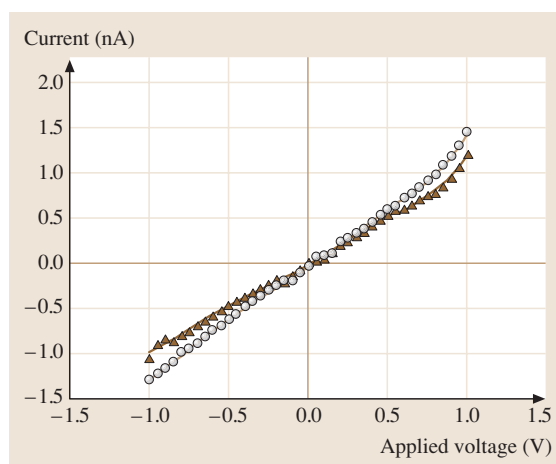


Fig. 54.4 Dark- (triangles) and photoconduction (circles) through spun NiPc films

the weak interaction of molecules. The film surface was also rough. The high nucleation rate of CuTTBPc on a silanized surface, on the contrary, produced a much smoother morphology consisting of densely distributed fine-grain clusters. The aggregation of the molecules took place in domains during the formation of the LB monolayer, separately distributed on the glass surface. These domains acted as active sites for the nucleation and growth of the later deposition process and high-density clusters were thus found in the early growth stage. X-ray diffraction (XRD) patterns demonstrated that the LB films grown on the glass substrate were more crystalline than those on other substrates [54.43].

The wet techniques, namely LB, spin coating and SA, are preferred to high-energy deposition because the deposition takes place at room temperature, reducing the possibilities of the chemical decomposition of the molecules caused by thermal damage. These deposition methods are considered below.

Langmuir–Blodgett (LB) technique

The LB method involves the transfer of individual Langmuir monolayers of amphiphilic molecules which self-assemble in an ultra-clean water subphase onto a suitably prepared solid substrate. An LB film, which may consist of a single or many layers, up to a depth of several visible-light wavelengths, are generally produced with fine control over the thickness and geometry to the precision at the molecular level. With the Y-

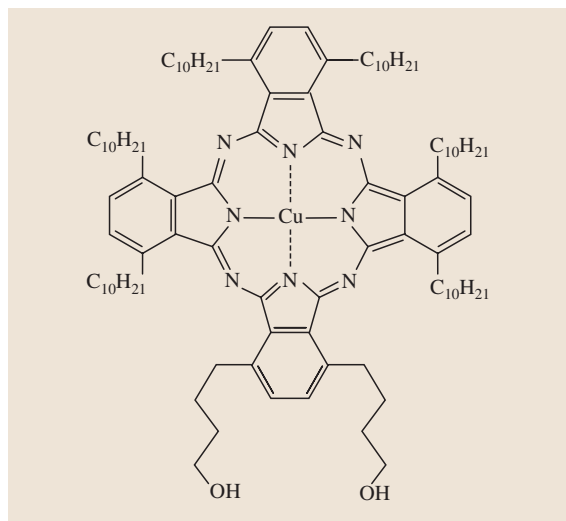


Fig. 54.5 Chemical structure of 1,4-bis(4-hydroxybutyl)-8,11,15,18,22,25-hexakisdecyl phthalocyaninato copper molecules

type construction, these LB films are essentially layered materials with alternating hydrophobic/hydrophilic regions. Non-centrosymmetric LB films can be obtained by X-type construction on immersion of the substrate from air into the water only, or Z-type deposition on withdrawal of the substrate from water to air [54.44].

Macrocylic molecules are not generally amphiphilic and are therefore not considered suitable for LB deposition. The synthesis of a series of specially designed Pc molecules for LB deposition has now been reported in the literature over the last two decades [54.45–47]. Figure 54.5 shows the chemical structure of asymmetrically substituted 1,4-bis(6-hydroxyhexyl)-8,11,15,18,22,25-hexa-octylphthalocyanine molecules belonging to this family of custom-designed molecules [54.48].

To start with LB deposition, a Langmuir monolayer is formed from a spreading solution of substituted Pc derivatives in an appropriate volatile solvent (such as chloroform) on the highly purified water subphase

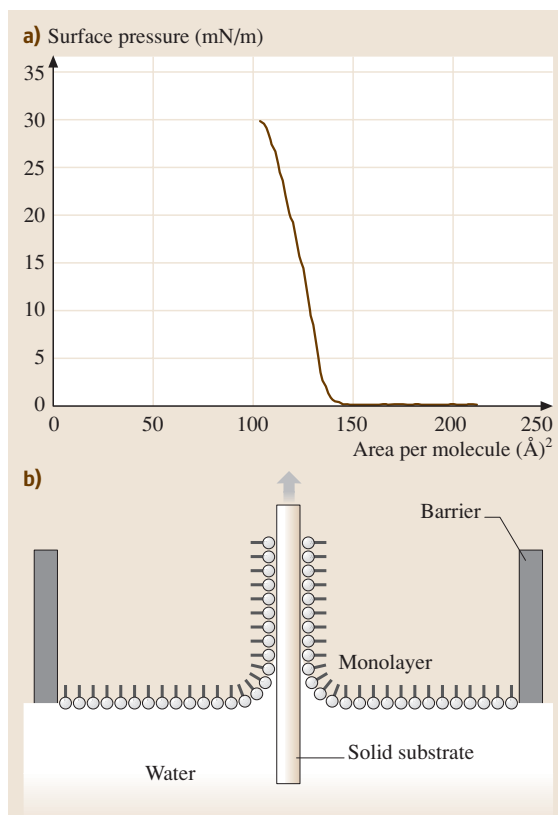


Fig. 54.6a,b Deposition of Langmuir–Blodgett film: (a) surface pressure–area isotherms and (b) transfer of floating monolayer onto a suitable substrate floating monolayer

(Milli-Q water of resistivity of 0.18 MΩ m) contained in an LB trough made of a hydrophobic material (teflon). The solvent is allowed to evaporate fully and the molecules are then slowly compressed to the desired organisation by closing a servo-controlled teflon barrier straddling the air/water interface at a constant speed (say about 100 mm/min). As shown in Fig. 54.6, the phase changes of the molecules during the compression are monitored by recording the surface pressure–area isotherm. The pressure begins to rise rapidly as the solid phase is reached while the area per molecule remains approximately constant. The molecules are transferred from the water/air interface to the substrate by dipping the substrate in at a constant speed of about 10 mm/min when the surface pressure is in the range 20–40 mNm⁻¹. However a dipping rate as high as 1000 mm/min was used to produce LB films of 5,10,15,20-tetrakis(3,4-bis[2-ethylhexyloxyphenyl])-21H,23H-porphine (EHO) molecules. Atomic force microscopy (AFM) showed a morphology of these films which is highly conducive to the host–guest interaction. The presence of isolated micron-size domains, which were themselves composed of grains of several nm in diameter, was observed [54.49].

The molecular orientation in LB films of these novel substituted Pc derivatives was investigated by spectroscopic methods, including electron spin resonance, reflection adsorption infrared spectroscopy (RAIRS), polarised infrared (IR) spectroscopy and AFM. Amphiphilic mesogenic Pcs afforded the best films. These all contained a good degree of molecular order; furthermore, the type of molecular stacking in the films was found to depend upon the length of the side chains and the central metal [54.50].

Spin-Coating Method

The spin-coating method, designed for defining patterns on silicon wafers in integrated circuit (IC) technology, has now been adapted for deposition of thin organic films on suitable substrates [54.51]. Substrates are vacuum held onto the rotating chuck of a photoresist spinner. The spread solution was prepared in the same way as done for the LB deposition and a small volume of the solution is dispensed onto the rotating substrate surface from a microsyringe held at a distance of 5 mm above the spinner platform. A spinning time of 30 s for a solution concentration of 0.5–5.0 mg/ml is found to be sufficient in order to produce a uniform, homogeneous film. The rotation speed is normally varied between 1000–6000 rpm and the speed of spin and the concentration of solution

largely determine the thickness of the resulting films. The dependence of the film thickness d on spin speed ω and time t may be written in terms of an empirical expression [54.52]:

$$d = \frac{C}{\sqrt{t}} \omega^{-x}, \quad (54.1)$$

where C depends upon the evaporation rate of the solvent, and the viscosity and density of the solution. The index x is predominantly determined by the evaporation rate of the solvent. If the evaporation of the solvent is independent of the spin speed, x takes on a value of 2/3. For most solvents used, the evaporation varies with $\sqrt{\omega}$ and x becomes 1/2. A value of $x = 1$ is a valid approximation for slow evaporation [54.53, 54].

Spin coating is a simpler and more cost-effective method than LB deposition and also there is no requirement for the molecules to be amphiphilic. The LB technique, however, provides more precise control over the film thickness [54.55]. Both spun and LB thin films of an octa-alkyl-substituted phthalocyanine molecules displayed similar characteristic features in their optical absorption spectra. The appearance of Davydov splitting and the XRD pattern indicated the same crystallinity of the films [54.56]. Different physical structure and molecular packing may result from the use of different wet techniques. For instance, asymmetrically substituted OC molecules (Fig. 54.5) were deposited by LB and spin-coating techniques. XRD patterns and UV–VIS spectra of these films indicated some degree of anisotropic ordering within the LB films compared to spun films [54.57]. The spin-coated films were, however, exceptionally smooth, even and free from crystallites. A noncompact spin-coated film of phthalocyanine molecules bearing one crown on ether ring exhibited faster response and reversal time than the well-ordered and tightly packed LB films [54.58].

Self-Assembled Monolayers (SAMs)

Self-assembled monolayers (SAMs) have attracted considerable interest because of their simplicity of preparation, stability and versatility. The introduction of due functional groups into SAMs allows changes of state and property on surface or interface. These attributes make SAM films attractive for the sensor technology [54.59, 60]. SAM films are formed via reaction of a functional group within a molecule with the surface of a solid substrate. The methoxy or trichlorosilylalkyl derivatives of molecules form weak bonds with hydroxyl groups and are suitable for the formation of a SAM on an oxide surface such as indium tin-oxide

(ITO) and glass (SiO₂) [54.61]. A monolayer layer can also be self-assembled on gold or silver substrates if the molecules are attached with thio or disulphides groups at one end [54.62]. In supramolecular aggregation during the self-assembly process, the interactions between the adsorbate molecules are as important as those between adsorbates and the surface. The size and aggregation pattern for the formation of supramolecular structures (J-aggregates) are controlled by changing the number of polar sulfonic groups of meso-tetra (4-sulfonatophenyl) porphine [54.63].

Much fundamental work on SAM films was initially undertaken with simple functionalised alkane derivatives [54.64]. In the case of alkylthiols on gold, it is well established that the monolayer films were densely packed with a high degree of order, with chains typically oriented at about 65° to the substrate surface. In recent years, work has been undertaken to include a single tether chain with thiol or disulphide derivatives for SAM formation on gold-coated glass substrates. The molecular orientation with respect to the gold surface was found to depend upon the different alkyl-connecting chain lengths and different macrocyclic peripheral side chains [54.65]. The core of substituted Pc molecules bearing mercaptoalkyl groups is not parallel to the surface if the tether chain is increasingly long. For sufficiently long tethers, the core becomes oriented almost normal to the surface [54.66]. SAM films of thiol-derivatised cobalt phthalocyanine complexes on gold electrodes was susceptible to destruction via oxidative and reductive desorption and their potential applications as a sensor were therefore limited [54.67].

Self-assembled ultrathin films have recently received considerable interest because they allow fabrication of supramolecular assemblies with tailored architecture and properties [54.68]. Multilayered films can also be built up by sequential deposition of polycations and polyanions based upon electrostatic attraction [54.69–71]. Alternate deposition of planar functional molecules meso-tetra (4-sulfonyl) porphyrin (TPPS₄) or copper phthalocyaninetetrasulfonic acid, tetrasodium salt (CuTsPc) and cationic bis (pyridinium) salt was made to produce a self-assembled multilayered film [54.72]. Multilayer assemblies of porphyrin and phthalocyanine were also prepared by alternating deposition of oppositely charged rigid planar molecules of sodium (phthalocyanine tetra-sulfonate)cobalt Na₄[(CoTsPc)] and tetrakis(N,N,N-trimethyl-4-anilinium) porphyrin cobalt [(CoTAP)]Br₄ [54.73]. A further investigation of the C-11 Pc derivative SAM has shown that the monolayer film was stable, exhibiting no oxidation and

only minor orientation changes on the gold surface over a period of 24 months as determined by infrared and fluorescence spectroscopy. The long active life of the Pc SAM was thought to be due to the macrocyclic ring possibly preventing oxidation of the thiolate root [54.74].

54.3.2 Thin-Film Properties

Surface/interface composition at the nanometre scale is believed to affect the organisation and chemical/physical properties of organic thin films. This long-range organisation determines both the optical and electrical properties of thin-film materials, leading to unique, new chemical sensor platforms. The overlap of π -electron wave functions from Pc molecule to Pc molecule is likely to occur between adjacent stacks in a thin-film form, giving rise to the broadening of energy levels [54.75].

Phthalocyanine Films

Phthalocyanines can exist in different polymorphic forms: α and β are among the most common. Both forms possess the herringbone structure for the stacking arrangement. The angle between the stacking axis and the normal to the molecular plane depends upon the method of preparation, types of phthalocyanine (metallo or metal-free) and substituents. For example, this angle is generally 25° and 45° for the α and β phases, respectively [54.76]. A typical absorption spectrum in the UV–visible range is shown in Fig. 54.3 for a substituted metal-free phthalocyanine (HPc) deposited on a glass substrate (similar to one shown in Fig. 54.2). The Q absorption band of the LB film was broader than one for the chloroform solution and appeared at the wavelengths between 650–800 nm. The Davydov splitting became apparent when compared with the spectra for the molecules in chloroform. The film forming properties and the stack order were both found to be influenced by the chain length of the ring substituents [54.77, 78]. An analysis into the in-plane molecular arrangements in the LB films of Pc compounds with short and long alkyl chains was performed by decomposing the absorption spectra into Gaussian–Lorentzian components. Long-chain molecules were found to be organised in a herringbone structure leading to the Davydov splitting of the Q-band. For short-chain molecules, the largely broadened blue component of the Davydov doublets was suppressed possibly due to the domination of an anisotropic stack-like molecular arrangement in LB films [54.79]. Characteristic Q-bands observed at about 630 nm in the UV–VIS spectra of the self-assembling monolayers (SAMs) of 2,9,16-Tri(tert-butyl)-23-(10-

mercaptodecyloxy)phthalocyanine and its disulfide on gold substrates were broadened and blue-shifted relative to those observed in solution [54.80]. The formation of high-quality Langmuir–Blodgett films of copper and nickel phthalocyanine derivatives substituted with short branched chains is reported. Ellipsometric and polarised optical absorption measurements suggest that the phthalocyanine molecules have a preferred orientation, with their large faces perpendicular to the dipping direction and to the substrate plane [54.81].

Electrical properties of **Pc** molecules are very dependent upon the doping and the nature of the substituents in the macrocyclic. Copper(II) tetrasubstituted phthalocyanine complexes, **CuPcX** (where $X = -\text{NO}_2$, $-\text{NH}_2$, $-\text{SO}_3\text{H}$, and $-\text{OH}$) exhibited an improvement of conductivity by five orders of magnitude over its unsubstituted counterpart. Further enhancement in conductivity was achieved by iodine doping. This increase in conductivity was attributed to the possible decrease in the metal–metal bond distance [54.82]. The effect of oxygen on charge transport was investigated by measuring the time-dependence behaviour of the film conductivity of zinc **Pc** (**ZnPc**) layers at a stable pressure of about 0.1 mbar of air and it was found that the conductivity gradually decreased by an order of magnitude with time. The conductivity reached saturation within several minutes for the film thickness smaller than 500 nm whereas similar electrical degradation in a 7- μm -thick film required more than half an hour. This thickness-dependent decrease in conductivity was caused by the velocity of the oxygen out-diffusion processes in the films [54.83]. The effect of doping on conductivity of a thermally deposited composite film of α -nickel phthalocyanine (**NiPc**) and the strong electron acceptor tetracyanoquinodimethane (**TCNQ**) was investigated by exposure to air. The doping took place at a much faster rate in the composite than in **NiPc** films. Values of 1.3 eV and 1.9 eV for the activation energy were obtained for devices incorporating **TCNQ** and the non-**TCNQ** devices, respectively, and the conductivity of the composite film was therefore found to be 20 times larger than the **NiPc** film [54.84]. Due to the excellent ability to photogenerate free charge carriers, the conductivity of the metal phthalocyanine (**MPC**) film is increased considerably as it can be seen from Fig. 54.4 showing the dark and illuminated current–voltage characteristics of a 10-nm-thick spun nickel phthalocyanine (**NiPc**) sandwiched between two metal electrodes.

Phthalocyanines of rare-earth metals primarily occur in the form of bisphthalocyanines with a sandwich-type structure and the cation is eightfold coordinated to the

two macrocycles. One of these phthalocyanine rings is virtually planar while the other is significantly distorted [54.85]. The Q-band in the absorption spectra of spun films of substituted lutetium bisphthalocyanine molecules becomes broader and red-shifted compared to the molecules in chloroform solution. Heat treatment of the film at temperature above 120 °C introduced molecular ordering, possibly due to the edge-to-edge interaction between neighbouring **Pc** moieties [54.86]. All these factors have led to successful formulation of phthalocyanines as chemically sensitive membranes for environmental monitoring [54.87–91].

Porphyrin Films

Inherent stability, unique optical properties and synthetic versatility of porphyrins and metalloporphyrins are exploited in sensor applications. Synthetic porphyrins and metalloporphyrins incorporated into polymers, glasses and Langmuir–Blodgett films matrices are used for detection of NO, CO₂ and O₂ because of the ability of heme to bind these gases. Metalloporphyrin sensing arrays have been used for the detection of organic odourants, such as amines, thiols and phosphines [54.92]. Porphyrins also combine readily with metals, coordinating with them in the central cavity. Many gas sensors take advantage of analyte binding to the centre metal atom in the porphyrin ring and a detectable optical change occurs as a result. In particular sensing properties of iron, zinc, copper, nickel, and cobalt containing porphyrins have now been studied [54.93–96]. The porphyrin rings of a thiol-derivatised cobalt (II) 5,10,15,20-tetrakis (4-tert-butylphenyl)-porphyrin (**CoTBPP**) molecules were immobilised on the surface of a 4-aminothiophenol (4-ATP) self-assembled monolayer (**SAM**) on gold (111) by in situ axial legation. The reconstruction of the herringbone structure took place probably due to adsorption/desorption processes of molecules [54.97].

Substituents have considerable effects on the structure of porphyrin monolayers; for example the interaction between the porphyrins deposited on the **ITO** substrate without bulky tert-butyl groups was much stronger than that of the porphyrins with bulky tert-butyl groups [54.98]. Hybrid molecule-silicon capacitors were formed by attaching [5-(4-dihydroxyphosphorylphenyl)-10,15,20-trimesitylporphinatozinc (II)] porphyrin complexes to silicon oxide via a phosphonate linkage and the presence of multiple distinct peaks in electrical characteristics were associated with oxidation and reduction of the molecular monolayer [54.99]. Multilayered thin films of

porphyrins bearing bulky alkoxyphenyl substituents at two of the four meso-positions and phenyl phosphonates at the other two were deposited on the ITO substrates using the zirconium phosphonate linkage. Molecular aggregation was prevented by the addition of sterically demanding 2,6-di(n-hexoxy)phenyl substituents to the meso-positions of the porphyrin skeleton. The com-

pounds were able to form thin films without the presence of large molecular chromophore interaction relative to sterically unhindered porphyrins [54.100]. Highly conducting tetra-ruthenated cobaltporphyrin (Co (TRP)) and tetrasulfonated zincporphyrin (Zn (TPPS)) multi-bilayer films were prepared by electrostatically assembly for sensor applications [54.101]

54.4 Sensing with Phthalocyanine and Porphyrin

The interaction of reactive gases such as O₂, NO₂ and NH₃ with the phthalocyanine group of compounds has been shown to result in conductivity changes of these compounds. This effect was associated with charge transfer between the electron-donating phthalocyanine molecule and the electron-accepting gas [54.102].

54.4.1 Amperometric Sensor

The action of the oxidising gases O₂ and NO₂ and the reducing gases NH₃ and H₂ diluted in N₂ on the electrical conductivity of thin layers of zinc hexadecafluorophthalocyanine (ZnF₁₆Pc) and zinc phthalocyanine (ZnPc) was investigated. The conductivity ZnF₁₆Pc increased in the presence of NH₃ whereas ZnPc exhibits no sensitivity to this gas. The sensitivity to H₂ was higher for ZnF₁₆Pc than for ZnPc. This behaviour was related to the redox potentials of the two phthalocyanines [54.103, 104].

Response and recovery times for LB CuTTBPc films on platinum IDE are shown in Fig. 54.7 for different gas concentrations of 1–5 ppm. These times were determined from a model based upon the kinematics of adsorption and desorption of NO₂ gas molecules. It was found that recovery times were longer than response times, irrespective of gas concentration. The response time constant varied in the range 105–159 s. Repeated exposures to NO₂–air mixtures resulted in gradual degradation of reproducibility. The response was also believed to be influenced by the past history of the exposure of the sensor to the NO₂ gas, if the recovery time constant was longer than the switch-off time. These factors show that CuTBPC is a material that is suitable for fabricating a disposable *single-shot* NO₂ sensor for practical uses [54.105]. LB films of an asymmetrically substituted phthalocyanine, 1,4-bis (4-hydroxybutyl) 8,11,15,18,22,25-hexaethylphthalocyanine molecules showed selective responses to 1–5 ppm concentrations of NO₂ at the room

temperature. Moisture had no effect on the response because of the hydrophobic nature of the alkyl groups. Exposure to Cl₂, NH₃, SO₂ and CO at ppm levels produced no measurable response [54.106]. Further work on the LB films showed that the NO₂ response was larger for the LB film produced by dipping the substrate perpendicular to the electrode finger than those dipped parallel to the fingers. This preferential behaviour was attributed to the ease of conduction along the long chains [54.107]. LB films of meso,meso'-buta-1,3-diyne-bridged Cu(II) octaethylporphyrin dimer molecules were used to fabricate amperometric sensors operating temperature of 90 °C. LB multilayers were reported to be selectively sensitive to small concentrations of NO in air without being affected by the contemporary presence in NO₂, CH₄, C₂H₅OH and CO [54.108].

Thickness, operating temperature, doping and post-deposition treatment of sensing membranes all affect the sensor performance. Vacuum-deposited CuPc of thickness 50–400 nm onto gold IDEs on glass substrate were

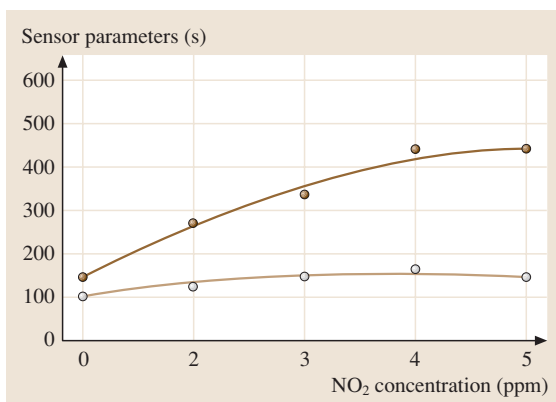


Fig. 54.7 Response (*broken line*) and recovery (*solid line*) of a 15-layer LB film of CuTTBPc when exposed to NO₂ periodically at 2-min intervals at 1, 2, 3, 4 and 5 ppm levels in succession

exposed to NO_2 gas of concentration 10–100 ppm. The film thickness had little effects on the room-temperature sensitivity, but the recovery ratio decreased with increasing film thickness. Thicker films showed improved recovery at 100 °C [54.109]. Due to the tetra-tert-butyl substitution on the periphery of phthalocyanine, **CuTTBPc** films have a larger lattice spacing, higher film resistance. Sublimed film **CuTTBPc** film showed a higher recovery ratio in the NO_2 sensing experiments [54.110].

NO_2 and O_2 treatment of evaporated **CuPc** films that were 160–200 nm thick on **IDE** improved the sensitivity and recovery time when exposed to 0.5–5 ppm of NO_2 gas. A Langmuir behaviour was predicted for the adsorption/desorption processes on the weakly binding surface sites of NO_2 -treated **CuPc** films having a single activation energy [54.111]. When the **CuPc** films were subjected to post-deposition treatment by cooling down to 77 K, the mechanism of NO_2 adsorption, however, followed the Elovich model [54.112]. 100-nm-thick **CuPc** and iron **Pc** (**FePc**) films were heat treated at 240 °C under vacuum and then the responses of the films to the exposure of NO_2 in the 8–12.8 ppm range were monitored. The **CuPc** films were transformed to a stable β -phase and the adsorption occurred on the ligand rings. NO_2 was, on the other hand, adsorbed on both the ligand ring and the central ion of the **FePc** films [54.113]. An amperometric sensor was fabricated using the spun film of tetra-iso-propoxyphthalocyaninato copper (II) (**i-Pro-CuPc**), and the response, recovery and cyclic properties of the sensor were very temperature sensitive. The results showed ideal gas sensitivity at 65 °C and a good linear relationship existed between the resistance of gas sensor and the concentration of NO_2 [54.114]. 25-nm-thick **NiPc** films were deposited between the source and the drain of a field-effect transistor (**FET**) and the change in the drain current exhibited a linear dependence on the ozone concentration in air, in the range 0–150 ppb [54.115, 116].

Water-soluble copper phthalocyanine tetrasulfonate (**CuTsPc**) molecules were alternatively self-assembled with a bipolar pyridine salt on a 3-mercaptopropionic-acid-modified Au electrode to produce copper ion-selective electrodes (**ISE**). These **ISE** were found to have low resistance, short conditioning time and fast response. The electrode potentiometric response showed selective potentiometric response to Cu^{2+} ion in the range from 1×10^{-5} – 1×10^{-1} M, independent of the pH of the solution between pH 1–5. The response was dependent on the nature of the medium and the detection limit was found to be 7×10^{-6} M in acetate buffer

(0.2 M, pH 4.5) [54.117]. Carbohydrates were detected by flow-injection analysis at the water-soluble cobalt phthalocyanine tetrasulfonate (**CoTsPc**)-modified electrode with high sensitivity. Detection limits obtained in this manner range from 150 pmol injected for glucose and fructose to 600 pmol injected for maltose and sucrose [54.118].

54.4.2 Optical Sensors

The amperometric approach generally suffers from long response times and their use is restricted due to possible fire and explosion hazards caused by electrical power. Organic systems are also prone to slow degradation arising from the chemical reactivity of charge carriers. Optical transduction techniques, on the other hand, offer high speed, high precision, immunity to interference, and remote sensing capabilities for detection of trace gas species.

Optical Absorption and Fluorescence Spectra

Optical transmittance of thermally evaporated lead phthalocyanine (**PbPc**) and nickel phthalocyanine (**NiPc**) thin films changed on exposure to NO_2 in the **IR** region of the optical absorption spectrum [54.119]. The disappearance of Davydov splitting from the **UV-VIS** absorption spectra of 20-layer-thick **LB** films of 1,4-bis(4-hydroxybutyl)-8,11,15,18,22,25-hexakisdecyl phthalocyaninato copper molecules was observed when

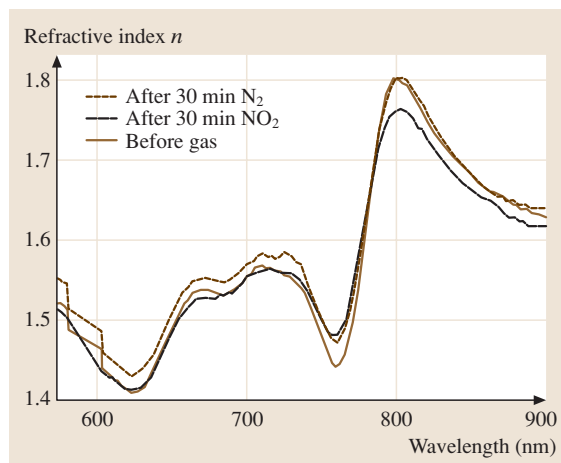


Fig. 54.8 The dependence of the refractive index of octa-substituted phthalocyanine on the wavelength before and after exposure to 90-ppm NO_2 gas for 30 min. The recovery was examined after flushing of the **LB** films with N_2 for 30 min

the films were exposed to 100 ppm of NO₂ [54.120]. The local interaction between the central metal atoms and NO₂ distorted the herringbone structure. Gas adsorption and desorption processes were described by exponential functions, both characterised by a single time constant. The dispersion relation in Fig. 54.8 for the refractive index was obtained by using simple Kronig–Krammer transform of absorption spectra of the LB thin film of another octa-substituted metal-free phthalocyanine molecules. The full recovery of the refractive index to its original value was achieved after flushing with the N₂ gas for wavelengths larger than 782 nm. Ellipsometry measurements on thin films of tetrasulfonated copper phthalocyanine showed increases in the real and the imaginary parts of the dielectric constant on exposure of NO₂ gas possibly due to the rise in the density of dipoles and higher absorption, respectively [54.121].

LB films of 5,15-bis(4-aminophenyl)-10,20-bis[3,4-bis(2-ethylhexyloxy)phenyl]-21H,23H-porphine were prepared at a dipping rate as high as 500 mm/min and an inhomogeneous structure was obtained with high porosity. These porphyrin films showed much faster response to 4.6 ppm of NO₂ gas and a sensitivity of 60% relative absorbance change at 439 nm was achieved. Full and accelerated recovery of the original spectrum was also achieved by gentle heating at 353 K. The sensor was reported to have a self-life as long as one year [54.122]. Kinetic UV–VIS spectroscopic measurements were made on a porphyrin-entrapped sol–gel film for NO₂ sensing. The method was capable of detecting levels as low as 176 ppb of NO₂ at room temperature and showed a fast and fully recovery [54.123]

The blue colour of rhodium phthalocyanine LB films becomes transparent upon chlorination. A pronounced quenching of the characteristic triplet centred on the Q-absorption band took place at 662 nm, but the absorption band in the near UV part of the spectrum remained almost unaffected. Optical spectra partially recovered when the exposed film was left in air for several hours. Overall effects of chlorination (quenching and recovery) depended on the period of exposure [54.124]. LB gadolinium phthalocyanine films were exposed to 10 ppm of chlorine and changes in optical absorption spectra were observed as a result of the oxidation of the film by chlorine to form [Gd(Pc)₂]⁺ species. The kinetics of such changes were described by a polyfunctional process with different decay time constants and the effects were found to be highly reversible [54.125].

SAM films are of interest because the chemically bound monolayer is intrinsically more robust than LB

films and the response times are also expected to be faster. Monolayers of diphthalocyanine disulfide Pc molecules were self-assembled on gold-coated glass substrates with the Pc macrocycle oriented parallel to the metal surface. Changes of the reflectivity signal were observed on exposure to NO₂ gas in proportion to the concentration [54.126]. The fluorescence emission spectrum of each of the Pc SAMs was obtained by exciting each monolayer along the longitudinal axis of the optical waveguide via laser-induced evanescent-wave stimulation. The use of the longer mercaptoalkyl connecting chain appeared to inhibit quenching of the electronically excited state through energy transfer to the metal layer. Fluorescence response to 10 ppm NO₂ was found to be selective with no interference from CO and CO₂ [54.127].

Surface Plasmon Resonance Technique

The surface plasmon resonance (SPR) technique is based on the excitation of surface electromagnetic waves of transverse magnetic (TM) modes travelling along the interface between a metal and a dielectric medium. Using a semicylindrical prism of high refractive index n_p in Kretschmann's configuration, as shown in Fig. 54.9, these waves are excited by a p-polarised light of wavelength λ via the evanescent field [54.128]. The evanescent field will be completely attenuated at a particular angle of incidence corresponding to resonance and there will be no reflection. Figure 54.10 shows the SPR results when a spun film of nickel(II) tetrakis(4-cumylphenoxy)phthalocyanine (NiPc) molecules was subjected a sequence of exposure to ozone (O₃) at 2 ppm. The period of 20 mins was allowed for the film to recover to its original state. The shift of the resonance angle $\Delta\theta_a$ was believed to be caused by a change in the refractive index of the film due to the interaction of O₃. $\Delta\theta_a$ is

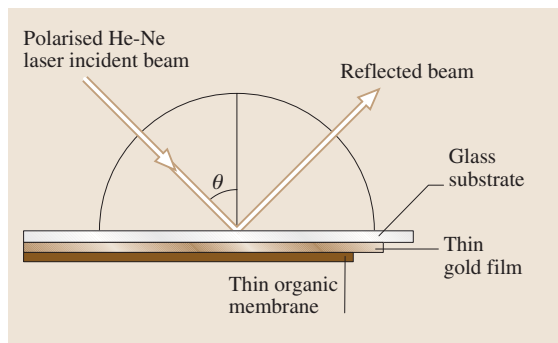


Fig. 54.9 A Kretschmann-type configuration to measure SPR data of CA thin films

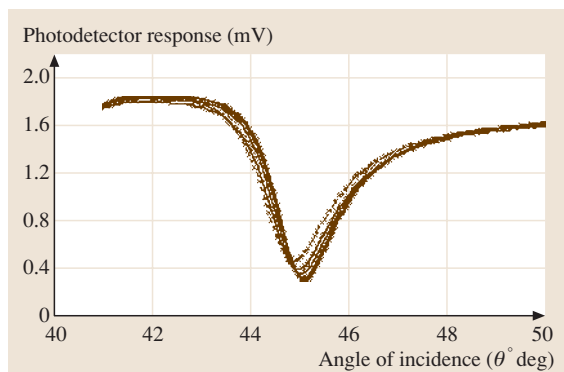


Fig. 54.10 The effect of a sequence of exposure at 20-min intervals of 2-ppm O_3 on a NiPc spun film. The broken line represents the system prior to exposure

usually written in the form [54.129]:

$$\Delta\theta_a = \frac{(2\pi/\lambda) (|\varepsilon_m| \varepsilon_i)^{3/2} d}{n_p \cos \theta (|\varepsilon_m| - \varepsilon_i)^2 \varepsilon} (\varepsilon - \varepsilon_i), \quad (54.2)$$

where $|\varepsilon_m|$ is the modulus of the real part of the dielectric constant of the gold film; ε_i is the dielectric constant of the medium (air in this case) in contact with the organic thin layer of thickness d and the dielectric constant ε . The resonance minimum moved to an increasingly larger angle after each exposure to ozone. The half-width became narrower at the same time and this was believed to be the consequence of oxidation of the phthalocyanine ring by ozone, which resulted in bleaching of the dye. SPR responses are in general slower and less readily reversible than semiconductor changes but the technique is capable of providing additional information on the interaction between the gas and films as the shifts in both the angle and depth of the resonance can be monitored. Experimental data from the SPR response of CuPc films to nitrogen dioxide were input to a design process using an evolutionary algorithm. 25-nm-thick gold layers were found to exhibit 42.9% greater contrast than layers with a thickness of 50 nm. Using evolutionary design predictions, further modifications could be tested for available materials, and redundant layers might be eliminated. By inclusion of the external optics, a design could be selected to accommodate poor precision ($\pm 0.5^\circ$) in the incident angle and a possible multi-layer solution was shown using Teflon AF 1600, with a refractive index similar to 1.3. The predicted NO_2 response showed an improvement compared with the classical SPR configuration, and the incident angle chosen by the genetic algorithm for the interrogation of these

layers was close to a stationary point in the absolute response curve [54.130].

Figure 54.11 shows the transient response when thick films of copper hexadecafluorophthalocyanine ($CuPcF_{16}$) were exposed to 100 ppm of NH_3 for 2 min followed by the injection of dry air for a further 2-min period. The film was exposed to 200 ppm of NH_3 for the next cycle. The SPR response was very rapid and the recovery was complete. Unsubstituted CuPc was practically insensitive to this gas. Strong electron-withdrawing fluorine substituents made this substituted compound sensitive to reducing gases such as NH_3 [54.131].

SPR experiments were performed on films of different phthalocyanine derivatives in order to investigate the interaction mechanism with NO_2 . SPR signal concentration as low as 1 ppm was measured using spun films of crown-ether-substituted phthalocyanines and octa-3,7,11-trimethyldodecyloxy phthalocyanine [54.132]. Adsorption of NO_2 took place both on the surface of the film and into the bulk. The surface adsorption increased the film thickness while the change in the real part of the film refractive index occurred due to the diffusion of NO_2 into the LB film. These processes were reversible and had no effect on the optical absorbance of the LB film. The SPR response of the bare Ag film to the exposure of NO_x (the equilibrium mixture of nitrogen dioxide and dinitrogen tetroxide) was slightly slower than the LB films of tetra-4-tert-butyl-phthalocyanitosilicon dichloride (tb-PcSiCl₂/Ag) system. This effect was associated with the high affinity of the phthalocyanine to NO_x

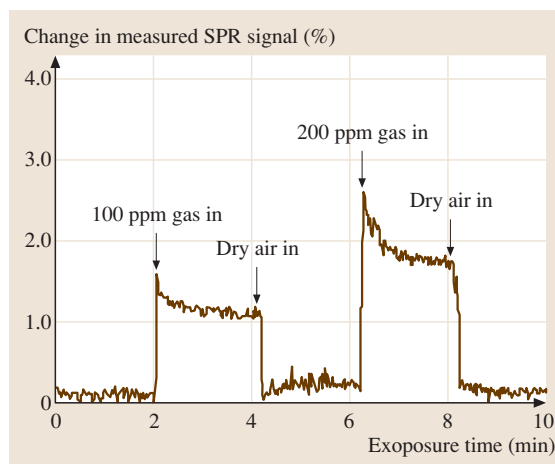


Fig. 54.11 Kinetics of the SPR response of copper hexadecafluorophthalocyanine ($CuPcF_{16}$) film to NH_3 gas at 100 ppm and 200 ppm. Measurements were at a fixed angle of $\theta^* = 46^\circ$

gas. The NO₂ gas was also able to reach the Ag/Pc interface film and the reaction with the metal film resulted in the growth of a surface layer. This irreversible effect was found to be predominant during the recovery cycle and considerably reduced by the presence of a buffer LB layer of ω -tricosenoic (ω -TA) acid [54.133]. SPR studies showed that exposure of thin films of 18-crown-6 metal-free phthalocyanine molecules to NO₂ decreased the film absorbance. The optical permittivity of the NO₂-treated Pc over-layer was regarded as being an average of the optical permittivities of both components since the optical fields associated with surface plasmon polaritons sampled both the Pc and the NO₂ molecules. The disruption in the charge conjugation of the phthalocyanine molecules was observed because of the generation of organic radical cations as end products of the charge transfer during the physisorption process [54.134].

Using the excitation at wavelengths of 488 and 632.8 nm, SPR measurements were made on LB films of porphyrine molecules of EHO type deposited on an Ag-coated glass substrate. The resonance shift observed was larger at 488 nm than at 632.8 nm when the EHO films were exposed to NO₂ gas. The thickness and the complex dielectric constants at 632.8 nm were attributed to the island structure of the EHO LB films but the derived properties at 488 nm were believed to be caused by dispersion due to optical absorption [54.135]. Similar results were further obtained from UV-VIS absorption in these films [54.49].

54.4.3 Detection of Volatile Organic Vapour Compounds

Phthalocyanine molecules have also been extensively investigated for the recognition of volatile organic compounds (VOC). Langmuir-Blodgett (LB) and evaporated films of lutetium bisphthalocyanine (LuPc₂) molecules were deposited on indium tin-oxide (ITO) interdigitated electrodes in order to study the changes in their conductivity at room temperature due to the presence of a variety of organic vapours with different chemical functionalities. The results demonstrated the viability of the phthalocyanine thin films as the active species for systems specifically designed for the monitoring of aromatic components in food. The majority of the work on vapour sensing has, however, been based upon quartz crystal microbalance (QCM) transduction techniques. The frequency shift Δf from the nominal resonance frequency f_0 of the crystal due to the change in the mass Δm due to the adsorption of the vapours

is [54.136]:

$$\Delta m(\text{mg}/\text{cm}^2) = \frac{\Delta f(\text{Hz})}{2.26 \times 10^{-6} f_0^2}. \quad (54.3)$$

It was demonstrated that monomeric soluble transition-metal phthalocyanines R₄PcM (R=tert-butyl or 2,2-dimethyl-3-phenyl-propoxy) used as sensitive coatings for quartz microbalance transducers show reversible interaction and high sensitivity for organic solvents with high boiling point [54.137]. Quartz microbalance devices coated with LB films of copper(II) tetra-(tert-butyl)-5,10,15,20-tetraazaporphyrin exhibit good sensing response to the vapour of benzene and toluene at room temperature [54.138]. Soluble tetrakis-hexyl- and dodecylthiophthalocyaninato nickel(II) and the corresponding Pd(II) and Ag(I) complexes were investigated as sensitive materials for the detection of organic solvent vapours using quartz microbalance and interdigitated capacitance transducers. Sensor responses were found to be reversible at room temperature with response times on the order of several seconds depending on the partition coefficients of the organic solvents in the phthalocyanine film [54.139]. LB films of lanthanide diphthalocyanines such as praseodymium, ytterbium as well as octa-tert-butyl praseodymium diphthalocyanines were known to display spectroscopic changes when exposed to tobacco smoke [54.140]. The sensitivity and partition coefficient for ethanol, dichloromethane, acetone, and *n*-hexane were found to be larger for the QCM sensor using thermally annealed ordered membranes of octa(13,17-dioxanonacosane-15-sulfanyl)-substituted mesomorphic nickel(II) phthalocyanine molecules than as-coated untreated films. It was found from Raman spectroscopy that molecules with saturated C-C bonds such as ethanol interact with phthalocyanine films predominantly by the formation of hydrogen bonds and the sensor response to π -bond-containing compounds such as acetone is the result of their π - π interaction with the conjugated phthalocyanine ring [54.141].

Changes in refractive index of lutetium bisphthalocyanine (LuPc₂) in the presence of ethanol, hexanal, *n*-butyl acetate and acetic acid were successfully exploited to produce an optical-fibre sensor operating at the wavelength of 1310 nm, capable of monitoring changes up to 10 dB in the reflected optical power for the detection of an 88-mmol/l concentration of acetic acid [54.142]. UV-VIS spectra of spin-coated layers of 29H,31H-(2,4-di-*t*-amylphenoxy)phthalocyanine, Zn(II) tetra-4-(2,4-di-*t*-amylphenoxy)phthalocyanine and Zn(II) tris-(2,4-di-*t*-amylphenoxy)-[4-(4-mercapto

-phenylimino-methyl)-phenoxy] phthalocyanine were found to be sensitive to tert-butylamine, diethylamine, dibutylamine, 2-butanone and acetic acid. The selectivity was determined by both the metal and the peripheral substituents [54.143]. The synthesis of specially designed bisphthalocyanine derivatives for VOC detection has been reported and their UV spectra are selectively sensitive to vapours depending on both the metal and the peripheral substituents. This observation has led to the fabrication of an *electronic optical nose* using an array of as-manufactured sensors for the analysis of some volatile organic compounds (VOC) that are of interest in food analysis [54.144].

The electrical conductivity of sol-gel-derived spun hybrid cobalt porphyrin-SnO₂ thin films showed fast and reversible response to methanol vapours; the highest responses were observed at 250 °C. The porphyrin was thermally stable up to 300 °C within the SnO₂ ma-

trix and enhanced the methanol detection sensitivity at lower working temperatures. The incorporation of porphyrin into SnO₂ film had no effect on the detection of CO [54.145]. Hybrid thin films were produced using porphyrin and phthalocyanine and the response of absorption bands of the blend systems to the presence of VOCs was different from that obtained with a single compound [54.146].

Toluene vapour sensing has been successfully demonstrated using LB films prepared from copper tetrakis-(3,3-dimethyl-1-butoxycarbonyl) phthalocyanine (CuPcBC), copper tetrakis-(3,3-dimethyl-1-neopentoxycarbonyl) phthalocyanine (CuPcNC) and nickel tetrakis-(3,3-dimethyl-1-butoxycarbonyl) phthalocyanine molecules. Exposure to toluene resulted in a partially reversible shift in the resonance depth and position of the SPR curves and toluene could be detected down to at least 50 ppm [54.147].

54.5 Polymeric Materials

A polymer comprises of repeating molecules with the same chemical structure. The electrical conductivities of the intrinsically conducting polymer systems now range from 10⁻¹⁰–10⁻⁵ S/cm. The common electronic feature of pristine conducting polymers is the π -conjugated system, formed by the overlap of carbon p_z orbitals and alternating carbon-carbon bond lengths. Doping of the polymers can increase the conductivity to as high as 10⁺⁴ S/cm, a value comparable to that of a metal.

54.5.1 Conducting Polymers

Figure 54.12 shows the chemical structure of a few commonly used conducting polymers such as polyaniline, polypyrrole, and polythiophene for chemical sensors. In addition to the deposition techniques described earlier, conducting sensing filaments were produced using the scribbling and platinum-wire techniques [54.148]. Sensing membranes were also formulated by laser-induced chemical vapour polymerisation [54.149].

LB films of stearic acid, a polyaniline oligomer (16-mer) and polypyrrole were deposited on the IDEs. Composite films of polyaniline and polypyrrole mixed with stearic acid in equal ratio by weight were also deposited on similar electrodes. Different brands of min-

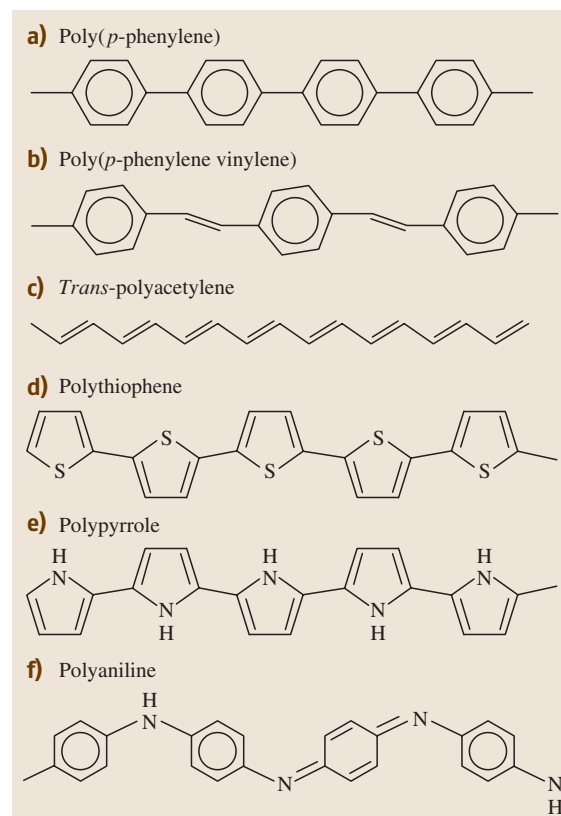


Fig. 54.12 Chemical structures of typical conducting polymers for sensors

eral water, tea and coffee were sensed by impedance measurements on the films over the frequency range of 20–10⁵ Hz. The sensor arrays composed of these films were able to differentiate tastants below the human detection threshold [54.150]. The Brunauer, Emmett and Teller (BET) surface area for an amperometric polyaniline/Au/Nafion[®] sensor prepared by the cyclic voltammetry (CV) method was found to be higher than structures prepared by the constant current (CC) method; the maximum sensitivity of CV-fabricated NO₂ gas sensors was 3.04 μA/ppm [54.151].

The type of doping is known to influence conducting-polymer-based sensors. Composite polyaniline emeraldine salts doped with an inorganic metal complex dopant, chromium(III) trioxalate (CTO) were produced by the chemically oxidative polymerisation method. Polyanilines were also electrochemically doped with naphthalene-1,5-disulphonic acid (NSA). The conductivities of these materials were monitored by using the four-probe method when pellets of these materials were exposed to several saturated vapours of organic solvents for 30 min; the results are summarised in Fig. 54.13. The conductivity of the CTO-doped pellets was reduced by 18% on exposure to CH₂Cl₂ whereas the exposure had no effect on NSA-doped material. The response of undoped composite polyaniline salt to CH₂Cl₂ was also very small. NSA-doped pellets, on other hand, showed a significant change in conductiv-

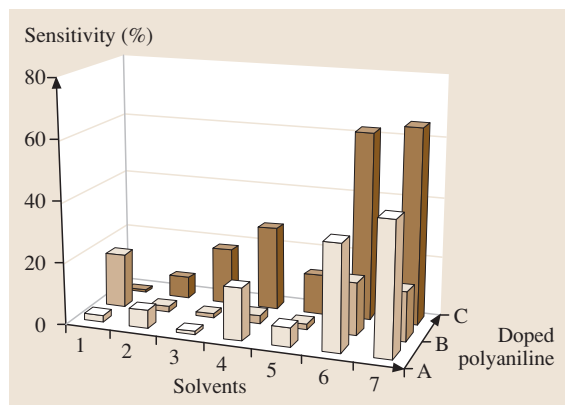


Fig. 54.13 Effects of vapour of: (1) dichloromethane (CH₂Cl₂), (2) chloroform (CHCl₃), (3) carbon tetrachloride (CCl₄), (4) acetonitrile (CH₃CN), (5) methanol (MeOH), (6) dimethylsulfoxide (DMSO), and (7) N-methylpyrrolidone (NMP) on the conductivity of: (A) pristine polyaniline emeraldine salt, and the salt doped with (B) chromium(III) trioxalate (CTO), and (C) naphthalene-1,5-disulphonic acid (NSA)

ity on exposure to CCl₄, while only very small changes were observed for the two other polymers. The responses to dimethylsulfoxide (DMSO) and N-methylpyrrolidone (NMP) were consistently higher for all three materials than the responses to the solvents CH₃CN and methanol (MeOH). It became apparent that the interaction of solvents with the polyaniline salt became stronger with increasing polarity of the solvents. The response was reversible for all three materials. The nature of the dopant in the material and the consequent change in polarity, especially at the dopant site, and the resultant effect on π -electron delocalisation and conductivity are primarily responsible for the characteristic sensing ability of the materials [54.152]. Extruded polymer blends containing polyaniline doped with dodecyl benzene sulfonic acid were dispersed in polystyrene (PSt) matrix filaments and the electrical conductivity of these filaments increased by a few orders of magnitude when exposed to a homologous series of alcohols, including methanol, ethanol and 1-propanol. The effect was reproducible and recovery was satisfactory. The sorption of analyte molecules was believed to facilitate conduction through the insulating PSt moieties by enhancing charge-carrier mobility through hopping processes between adjacent polyaniline particles [54.153].

Multilayered thin films of polypyrrole were prepared by modifying a preformed Langmuir–Blodgett (LB) film of stearic acid by exposure to gaseous reactants such as hydrochloric acid and pyrrole vapours. A change in the electrical resistance of the film was observed when the film was exposed to polar molecules such as methanol, ethanol and acetone, while the effect of nonpolar molecules on the resistivity of the film was found to be smaller. The response of LB films to exposure to ethanol was faster than that of electrochemically deposited polypyrrole, possibly due to the high ratio of surface area to bulk volume in the LB film [54.154]. Changes in mass and conductivity of polypyrrole thin films were measured to sense the primary alcohols [54.155].

Attempts have been made to integrate polyaniline optical sensor elements with optical communication technology for remote sensing by using 1300 nm as the operating wavelength. A 1% increase in transmission was observed at 1300 nm for electrochemically prepared polyaniline films when exposed to gaseous ammonia levels as low as 6 ppm at 50% relative humidity (RH). Different concentrations of ammonia were read by calibrating the sensors at intervals of 15 s. The response time was found to be insensitive to relative humidity variations in the range 30–70% [54.156].

Certain specially prepared polyaniline films showed partially reversible absorbance changes in the wavelength range 620–728 nm when exposed to 50–100 ppm of ozone at room temperature. The maximum sensitivity was attained at 620 nm. The cost-effective commercial exploitation of this effect was possible since the wavelength range was compatible with implementation on low-cost plastic optical fibres and small light sources [54.157].

Efforts have been invested in the use of information technology techniques to produce smart sensors. The sensor system, consisting of an acoustic two-port resonator operating at 433.92 and 380.8 MHz was configured as a frequency oscillator, including an integrated electronic module. The polymeric membranes were tested at room temperature for response to NO₂, NO, NH₃, CO, CH₄, SO₂, and H₂S in N₂. Responses to relative humidity (RH), and organic vapours (ethanol, acetone, and ethyl acetate) were also monitored. The sensitivity was found to be high. Principal component analysis (PCA) was performed to distinguish between different vapours of low concentrations [54.158]. Fluorescence emission from polymer-immobilised dye molecules on the multi-fibre tips was studied on exposure to organic vapours. Temporal responses were found to depend upon chemical nature (for example, polarity, shape and size) of both the vapour and the polymer; these were used as input signals to train a neural network for vapour recognition. The system was able to identify individual vapours at different concentrations accurately [54.159]. Similar work was reported using the solvatochromic dye, Nile red. The dye was immobilised within various polymers. The substrate played a role in determining the sensitivity of the sensor. The sensitivity attained with microstructure glass (MSG) substrates was seven times greater than that with SU-8 photoresist-coated glass substrate and a 50% faster recovery was also achieved with the MSG substrates. The MSG sensor array was able to fingerprint the response for separate analytes with a high degree of repeatability. Using pattern-recognition techniques, sensor arrays were adaptable for gas identification and discrimination ([54.160]).

54.5.2 Ion Sensing

Water purification requires calibration of metal-ion contents. Polymeric ion-selective electrodes (ISEs) for Pb²⁺ incorporating *N,N'*-bis(salicylidene)-2,6-pyridinediamine with 2-nitrophenyl octyl ether and 50 mol % lipophilic additive were reported to have rapid response and excellent selectivity towards lead

ions over other interfering metal ions [54.161]. *N,N'*-bis(5-methylsalicylidene)-*p*-diphenylene methane diamine formed a complex with Pb²⁺ and its selectivity was high, possibly due to the fact that the distance between the two nitrogen atoms and the position of the two hydroxyl group is matched with the size of Pb²⁺ ions. ISEs based upon a dispersion of this Schiff base compound into the polyvinylchloride (PVC) membrane were characterised by a fast response time, a wide linear dynamic range and a fair selectivity coefficient with a slope of 29.4 mV per decade. The sensor had a low detection limit and an active life of three months without displaying considerable divergence in potentials [54.162]. A cleaned gold microelectrode was soaked in the freshly prepared solution of *o*-amino thiophenol (*o*-AT) and the metal nitrate of Cu, Hg and Pb in *N,N*-dimethylformamide (DMF) for 4 h at room temperature. Simultaneous interaction took place between the thiophenol group of *o*-AT and the gold surface and its thiophenol and amino groups and M²⁺. The ratio of 4 : 1 was found to be appropriate for *o*-AT:M²⁺ for the self-assembly of the *o*-AT on the gold surface and the formation of recognition cavities. The prepared ISEs showed specific selectivity to the template metal ions in mixed solutions containing the three heavy-metal ions. The limits of detection for ISEs were found to be 1.46 × 10⁻⁸ M, 3.73 × 10⁻⁸ M and 4.34 × 10⁻⁸ M for Hg⁺⁺, Cu⁺⁺ and Pb⁺⁺ ions, respectively [54.163]. Membranes containing five-layer LB films of tetracarboxylic perylene derivative and polypyrrole molecules were able to detect trace levels of Cu²⁺ ions in water [54.164]. The thiol-Cu-SAM particles were doped by the adsorption of thioxyleneol or decanethiol into the porous polypyrrole film surface, resulting in an improvement in the sensitivity of the film to NH₃ [54.165]. Water-soluble regioregular polythiophenes containing acid C side chains were found to be suitable for the development of new Zn²⁺, Mn²⁺, and Cd²⁺ sensors [54.166].

54.5.3 Examples of Other Polymeric Sensors

A coordination polymer poly(CuMBSH) was formed via reaction of the bifunctional amphiphilic ligand, 5,5'-methylenebis(*N*-hexadecylsalicylideneamine) and copper ions at the water subphase. The response of LB films of poly(CuMBSH) to exposure of benzene, toluene, ethanol and water was monitored by SPR measurements. The film became swollen, possibly due to the diffusion of solvent vapour into the polymer film. Poly(CuMBSH) is regarded as a relatively nonpolar ma-

terial and its interactions were expected to be greater with vapours having a smaller dipole moment; the sensitivity increased with smaller dipole moment and higher refractive index of the vapour. The refractive index of the film increased because of an increase in the film density with the vapour filling the free volume inside the film. Similar results were obtained from admittance spectroscopic measurements on the same organic systems [54.167, 168].

The electrical properties of poly(methyl methacrylate) polymer (PMMA) films have been exploited for sensing applications (see Fig. 54.14a for the chemical formula). An increase in resistance of up to three orders of magnitude was observed for composite thin films of PMMA with carbon nanotubes when exposed to dichloromethane, chloroform and acetone. The sensing mechanism is explained on the basis of volume expansion and polar interaction of various vapours on

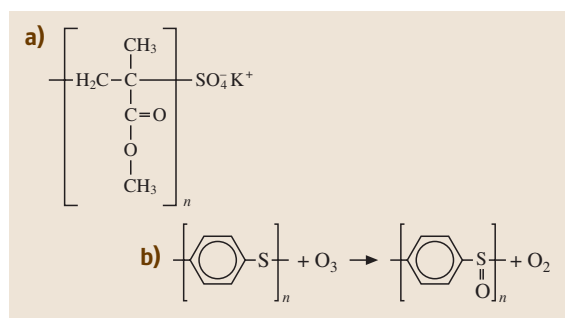


Fig. 54.14a,b Chemical structures of (a) poly(methyl methacrylate) derivatives and (b) reaction of polyphenylsulfide molecules with ozone

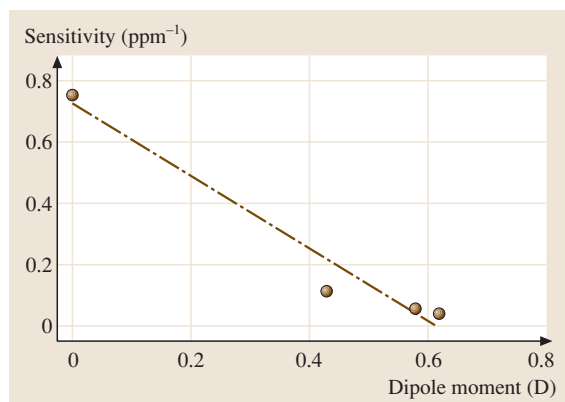


Fig. 54.15 Response of spun PMMA films on exposure to benzene (0 D), toluene (0.43 D), ethyl benzene (0.58 D) and m-xylene (0.62 D)

the nanotube surface [54.169, 170]. SPR measurements were made to investigate the room-temperature response of spun PMMA films to benzene, toluene, ethyl benzene and m-xylene (BTEX) vapours under dynamic conditions. The response of PMMA to benzene was fast and reversible. The dissolution of benzene in the bulk of the polymer film formed a heterogeneous layer, primarily giving rise to swelling of the film and the value of the partition coefficient was estimated to be 112. Figure 54.15 shows that the increase in angular shift per ppm was linear with decreasing dipole moment of the solvent vapours. Benzene is a nonpolar solvent and toluene, ethyl benzene and m-xylene are expected to show stronger solvation than benzene. Dissociated solvent ions may have formed a shell of bound ions and, as a result, the effective radius for dissolution in the polymer matrix would have increased. This dissociation might not easily occur for benzene, producing the highest SPR response [54.171]. A sensor has been made from a permselective poly(dimethylsiloxane) (PDMS) hollow-fibre membrane, showing a fast response time, very high oxygen permeability, and optimised oxygen/nitrogen selectivity. This sensor was suitable for monitoring the oxygen content in the outlet stream generated by medical oxygen concentration units [54.172].

Single-polyaniline films generally suffer from poor mechanical stability and polyaniline-blend films were prepared for practical applications using PMMA and PSt. The presence of water vapour, functioning as the interference gas, led to the lowering of the NH_3 response of the sensor in a humid atmosphere. The humidity effect was larger for PMMA than the PSt blend film. The difference was, however, not as large as expected from the water-sorption ability of PMMA [54.173]. The detection limits of ISE membranes with solid contacts are generally lower than a traditional liquid inner contact because of the diminished ion fluxes. Poly(methyl methacrylate)/poly(decyl methacrylate) (PMMA/PDMA) copolymer was employed as a solvent-cast membrane matrix on a layer of poly(*n*-octyl)thiophene (POT) deposited on Au as the internal contact. Ca^{2+} - and Pb^{2+} -selective electrodes were not sensitive to O_2 and the presence of a water film between the membrane and the internal contact was not found. The limits of detection were better by an order of magnitude and the response at low concentrations was much faster than for the liquid-contact electrode. For example, the drift was found to be smaller than 0.4 mV/min after 2 min when the concentration was increased from 10^{-9} to $10^{-7.7} \text{ M}$ [54.174].

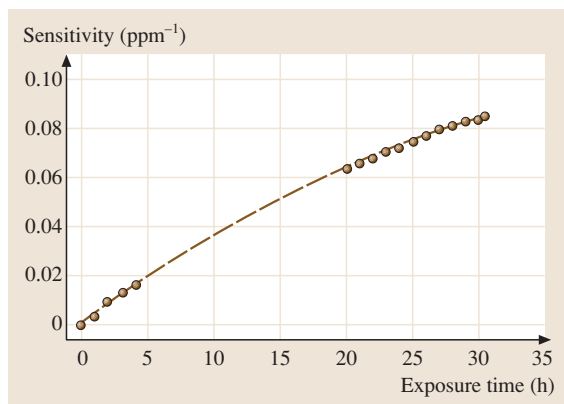


Fig. 54.16 Time-dependence behaviour of ozone sensitivity of PPS films. Two sets of hourly readings, separated by 16 h of continuous exposure without SPR measurements (*dashed line*)

An amperometric hydrogen sensor was proposed using a proton-conducting solid polymer electrolyte membrane (PEM), a blend of palladium and platinum as the anode and platinum as the cathode. The sensor operated as a fuel cell ($\text{H}_2/\text{Pd-Pt}/\text{PEM}/\text{Pt}/\text{O}_2$) and the short-circuit current was found to be linearly related to the hydrogen concentration [54.175].

It has recently been reported that thin films of polyphenylsulfide (PPS) (commercially termed noXon) act as efficient scrubbers of ozone from atmospheric ambient through the oxidation of the PPS molecules [54.176]. Thin films of this compound are found to be a useful material for the fabrication of

sensing membranes suitable for the detection of ground-level ozone at concentrations of a few ppm or even lower [54.177, 178]. A 1-h exposure to 2 ppm of O_3 was shown to cause at least a 1.1% change in the refractive index of the film [54.179]. As shown in Fig. 54.14b, oxidation of the PPS polymer by ozone exposure results in an irreversible increase in the index of refraction of the polymer [54.180].

Figure 54.16 shows the results of SPR measurements on PPS films when exposed to 1.5-ppm ozone. The increase in the refractive index Δn was found to be linear over the first few hours of exposure with an estimated slope of 1×10^{-4} refractive index units (RIU)/min. The sensitivity was defined as the ratio of Δn to the concentration of ozone. The interaction of O_3 with PPS films is believed to be an accumulative effect and such mechanisms can therefore serve as both a scavenger as well as an indicator of ozone in a certain ambient. The density of the binding of oxygen to a PPS film after five hours of exposure to 2-ppm ozone was estimated from QCM measurements to be about $5 \times 10^{18} \text{ cm}^{-3}$.

Electrospun nanofibers with diameters of 100–400 nm were deposited on the surface of a QCM by electrospinning homogenous blend solutions of cross-linkable poly(acrylic acid) (PAA) and poly(vinyl alcohol) (PVA). The NH_3 sensing properties were mainly affected by the content of the PAA component in the nanofibrous membranes, the concentration of NH_3 , and relative humidity. The sensitivity of nanofibrous-membrane-coated QCM sensors was also much higher than that of continuous-film-coated QCM sensors [54.181].

54.6 Cavitand Molecules

Thin films of some novel cavitand compounds such as crown ethers [54.182] and calixarenes [54.183, 184] can form inclusion complexes with some organic guest molecules. This effect is being extensively exploited for the development of sensors for organic vapours [54.185, 186]. Thin films can be prepared using LB film deposition, spin coating and self-assembly techniques [54.187–190]. The nanoporous flexible structure of thin LB films of amphiphilic calixresorcinarene derivatives are found to provide a suitable matrix for the incorporation of aromatic molecules [54.191]. This adsorption process was very fast, and full recovery of the film was observed after flushing with clean air. It has to be pointed out, however, that the detected vapours were

of a high concentration (a few percent by volume) and the adsorption was not selective since all vapours studied yielded a similar response. However, this may lead to the development of a sensor for explosives, where specificity is not considered relevant. These effects are attributed to weak and nonspecific interactions between the guest molecules and the calixarene LB film. It was also shown that the adsorption of organic vapours occurs in the whole bulk of the LB films, and that the number of adsorbed molecules is much higher than the number of calixarene molecules [54.192]. The adsorption mechanism involved the swelling of the film and even condensation of the adsorbate within the film. The swelling of the film was confirmed by independent

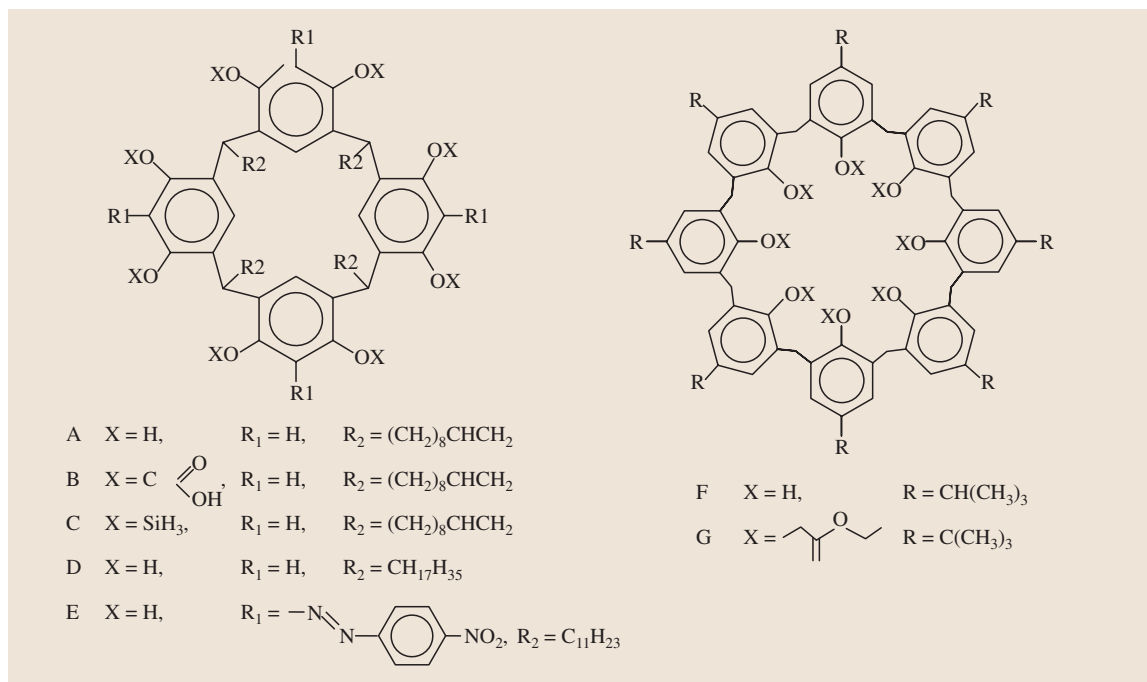


Fig. 54.17 Chemical formulae of calixresorcinarene derivatives

measurements using ellipsometric and surface plasmon resonance (SPR) techniques [54.193]; the adsorption mechanism remained still unclear. For all the studied analytes, the number of adsorbed molecules was found to be much larger than that expected from the geometrical dimensions of the intrinsic calixarene cavity and the empty space between the molecules. This discrepancy was explained by either film swelling or due to the condensation of vapour molecules inside the film, or both [54.191]. Spun films of calixresorcinarenes, however, were found to be homogeneous, and the porosity of the film was similar to that of LB-deposited films. Both LB and spun films of comparable thickness exhibited similar SPR response on exposure to toluene vapour [54.55]. Prolonged irradiation of the CA films with a focused laser beam caused an initial increase in film sensitivity to various organic vapours [54.194].

Figure 54.17 shows the chemical structure of an amphiphilic calixresorcinarene derivative with several different types of substituents. Exposures of layers of CAs to vapours of benzene, ethylbenzene, toluene and m-xylene in low concentrations produced changes in the optical properties, i. e., the film thickness and refractive index of the layers. Fast response and recovery processes have been observed, with response times as short as a few

seconds. The normalised SPR responses are shown in the three-dimensional (3-D) diagram in Fig. 54.18. It is apparent that the interaction of the analyte was, in general terms, specific to the thin film of a particular CA derivative. The adsorption mechanism was interpreted in terms of the accumulation of the vapour molecules in

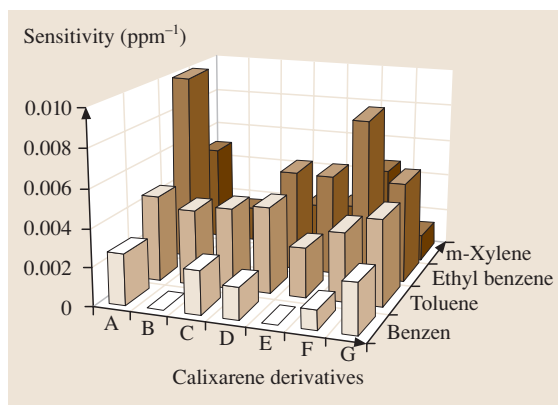


Fig. 54.18 A 3-D representation showing the response of different calixarene derivatives to different organic vapours (benzene (B), m-xylene (X), toluene (T), and ethylbenzene (E)) at a concentration of 375 ppm

the liquid phase inside the film matrix, probably caused by capillary condensation in the porous structure of the CA films [54.195]. These LB films had a characteristic pore size of about 1 nm. Condensation of vapour occurred inside capillaries similar to the porous structure of calixarene films at pressures lower than their saturated pressure at a certain temperature. The saturated vapour pressures of ethylbenzene and m-xylene are similar and therefore their exposure to the CA derivatives produced similar effects. Benzene on the other hand, with its highest saturated vapour pressure, yielded the smallest detectable SPR signal.

Composite LB films of amphiphilic CA and PPS were exposed to 2 ppm of O₃ [54.177]. The competition between the permanent oxidation process of the PPS polymer by the adsorbed O₃ molecules and the release of O₃ from the CA matrix was found to depend on the molar ratios of the CA and PPS compounds. Recovery became slower with lower CA proportions in the film matrix.

54.7 Concluding Remarks

The scope of organic materials for chemical sensing is huge and it is impossible to provide a complete description of these materials. Electronic artificial noses are being developed as systems for the automated detection and classification of odours, vapours and gases. These instruments consist of three main components: (i) an array of chemical membranes (ii) electronic circuitry for data acquisition, signal processing and display and (iii) a pattern-recognition algorithm. Up-to-date information on applications of materials for electronic noses and tongues is available in a recent review [54.197]. Problems associated with human senses are many: individual variability, impossibility of online monitoring, subjectivity, adaptation, infections, harmful exposure to hazardous compounds, and mental state. These limitations can be overcome by developing intelligent sensor systems. Gas sensors tend to have very broad selectivity, responding to many different analytes of varied concentrations. The electronic nose/tongue, therefore, offers a definite advantage in many applications in the food and utility industries, the health care and medical care sectors, and security services. The demand for advanced electronic noses will continue to stimulate the search for novel sensing materials.

Mathematical and computational tools are expected increasingly to play a part in the design of advanced

The conductivity of the CA derivative is intrinsically low. CA films were deposited on the gate between the source and the drain of a charge-flow transistor and the turn-on response for the transistor upon exposure to organic solvent was recorded. The increase in the membrane conductivity is partially attributed to condensation of the vapours in the highly microporous membrane even below the saturation vapour pressure and partially to the effect of the polar analyte molecules complexing inside and between the OH groups of the cavities. The technique offers several advantages over existing methods: (i) immunity to water vapour, due to the hydrophobic nature of the membrane; (ii) no catalytic poisoning of the membrane, as is commonly observed for doped SnO₂; (iii) no accumulative effects, which are responsible for baseline drift in quartz-crystal-type sensors, are observed, and (iv) no porous metal layer, the adhesion of which may be prone to degradation, is needed on top of the membrane [54.196].

electronic-nose systems. An electronic nose has been developed to monitor breathing air in human habitats. A molecular modelling study was undertaken to investigate the interactions between resistive sensors of a polymer-carbon black (CB) composite and analytes. Poly(4-vinylphenol), polyethylene oxide, and ethyl cellulose were considered for modelling, based on their stereoisomerism and sequence isomerism. The CB was modelled as uncharged naphthalene rings with no hydrogen. Molecular mechanical and molecular dynamics techniques were employed and the equilibrium composite structure was constructed by inserting naphthalene rings into the polymer matrix. The radial distribution profiles produced information on the composite microstructure. The sensor response was predicted in terms of the interaction energies of the analytes with the composites. Studies included both inorganic and organic analytes [54.198].

Research efforts are also growing in the mineralisation of VOC pollutants to innocuous compounds [54.199]. Visible-light-assisted removal of organic pollutants by photocatalytic action of dye-sensitised TiO₂ surfaces offers several attractive advantages. Firstly, the nanoscale device architecture is versatile with several methods of solar energy conversion whilst producing a chemical fuel in the form

of pure H₂. Secondly pollutant species and concentrations of mixtures in industrial waste streams can be identified [54.200]. Results so far reported are encouraging. For example, 40–75% degradation of aromatic pollutants such as phenol, chlorophenol, trichloroethylene and surfactants was achieved with TiO₂ surfaces modified by methylene blue and rhodamine B dyes af-

ter less than 5 h of irradiation with a 150-W xenon lamp [54.201]. Individual VOCs including methylene chloride, ethanol, benzene, acetone, xylene and isopropanol produced unique signatures as they were oxidised on the sensor surface [54.202]. Interest in hybrid hetero-supramolecular structures will therefore remain alive for the foreseeable future.

References

- 54.1 W. Gopel: *Sensors Actuat. B* **18-19**, 1–21 (1994)
- 54.2 M. C. Petty: *Biosens. Bioelectron.* **10**, 129–134 (1995)
- 54.3 M. J. Cook: *Chem. Rec.* **2**(4), 225–236 (2002)
- 54.4 L. Alcaer: *Conducting Polymers Special Applications* (Reidel Publications, Dordrecht, Holland 1987)
- 54.5 E. B. Feresenbet, E. Dalcanale, C. Dulcey, D. K. She-
noy: *Mol. Cryst. Liq. Cryst.* **397**, 585–594 (2003)
- 54.6 N. K. Hunt, B. J. Marinas: *Water Res.* **31**, 1355–1362 (1997)
- 54.7 T. Oshima, K. Sato, H. Terauchi, M. Sato: *J. Electrostat.* **42**, 159 (1997)
- 54.8 N. Carmona, M. A. Villegas, J. M. F. Navarro: *Sensors Actuat. A Phys.* **116**(3), 398–404 (2004)
- 54.9 N. Carmona, M. A. Villegas, J. M. F. Navarro: *Thin Solid Films* **458**(1–2), 121–128 (2004)
- 54.10 C. L. Baban, Y. Toyoda, M. Ogita: *Jpn. J. Appl. Phys.* **143**(10), 7213–7216 (2004)
- 54.11 I. Toma-Dasu, U. Dasu, M. Karlsson: *Phys. Med. Biol.* **49**(19), 4463–4475 (2004)
- 54.12 S. E. J. Williams, P. Wootton, H. S. Mason, J. Bould, D. E. Iles, D. Riccardi, C. Peers, P. J. Kemp: *Science* **306**(5704), 2093–2097 (2004)
- 54.13 F. Bender, C. Kim, T. Mlsna, J. F. Vetelino: *Sensors Actuat. B Chem.* **77**(1–2), 281–286 (2001)
- 54.14 B. Onida, L. Borello, S. Fiorilli, B. Bonelli, C. O. Areat, E. Garrone: *Chem. Commun.* **21**, 2496–2497 (2004)
- 54.15 S. Sen, K. P. Muthe, N. Joshi, S. C. Gadkari, S. K. Gupta, Jagannath, M. Roy, S. K. Deshpande, J. V. Yakhmi: *Sensors Actuat. B Chem.* **98**(2–3), 154–159 (2004)
- 54.16 B. H. Timmer, K. M. van Delft, R. P. Otjes, W. Olthuis, A. van den Berg: *Anal. Chim. Acta* **507**(1), 137–143 (2004)
- 54.17 M. Beekmann, G. Angellet, G. Megie, H. G. J. Smith, D. Kley: *J. Atmos. Chem.* **19**, 259 (1994)
- 54.18 L. Xie, T. J. Lu, H. Q. Yan: *Electroanal.* **10**, 842 (1998)
- 54.19 Th. Becker, L. Tomasi, Chr. Bosch-v. Braunmühl, G. Müller, G. Sberveglieri, G. Fagli, E. Comini: *Sensors Actuat. A Phys* **74**, 229 (1999)
- 54.20 H. Schulz, G. B. De Melo, F. Ousmanov: *Combust. Flame* **118**, 179–190 (1999)
- 54.21 B. Zielinska, J. C. Sagebiel, G. Harshfield, A. W. Gertler, W. R. Pierson: *Atmos. Environ.* **30**, 2269–86 (1996)
- 54.22 F. B. Reig, J. V. Adelantado, V. P. Martinez, M. C. Moreno, M. T. Carbo: *J. Molec. Struct.* **480-481**, 529–534 (1999)
- 54.23 W. Groves, E. T. Zellers, G. C. Frye: *Anal. Chim. Acta* **371**, 131 (1998)
- 54.24 W. A. Groves, E. T. Zellers: *Ann. Occup. Hyg.* **45**, 609–623 (2001)
- 54.25 N. Kasai, I. Sugimoto, M. Nakamuro, T. Katoh: *Biosens. Bioelectron.* **14**, 533–539 (1999)
- 54.26 G. Sberveglieri: *Sensors Actuat. B* **23**, 103–109 (1995)
- 54.27 D. Manno, A. Serra, M. Di Giulio, G. Micocci, A. Tepore: *Thin Solid Films* **324**, 44–51 (1998)
- 54.28 N. Taguchi: Japanese Patent Application No. 45–38200 (1962)
- 54.29 C. D. Kohl, A. Eberheim, P. Schieberle: *Tech. Mess.* **71**(5), 298–304 (2004)
- 54.30 A. Eberheim, D. Kohl, P. Schieberle: *Phys. Chem. Chem. Phys.* **5**(23), 5203–5206 (2003)
- 54.31 J. Gutierrez, J. Getino, M. C. Horriilo, L. Ares, J. I. Robla, C. Garcia, I. Sayago: *Thin Solid Films* **317**, 429–431 (1998)
- 54.32 M. Graf, D. Barretino, S. Taschini, C. Hagleitner, A. Hierlemann, H. Baltés: *Anal. Chem.* **76**(15), 4437–4445 (2004)
- 54.33 E. Comini, G. Faglia, G. Sberveglieri, Zhengwei Pan, Zhong L. Wang: *Appl. Phys. Letts.* **81**(10), 1869–1871 (2002)
- 54.34 A. Gramm, A. Schutze: *Sensors Actuat. B Chem.* **95**(1–3), 58–65 (2003)
- 54.35 O. K. Varghese, D. Gong, M. Paulose, K. G. Ong, C. A. Grimes: *Sensors Actuat. B Chem.* **93**, 338–344 (2003)
- 54.36 A. K. Prasad, P. I. Gouma: *J. Mater. Sci.* **38**(21), 4347–4352 (2003)
- 54.37 N. B. McKeown: In: *Phthalocyanine Materials. Synthesis, Structure and Function* (Cambridge Univ. Press, Cambridge 1998) p. 60
- 54.38 S. Tabuchi, H. Tabata, T. Kawai: *Surf. Sci.* **571**(1–3), 117–127 (2004)
- 54.39 M. Szybowski, T. Runka, M. Drozdowski, W. Bala, A. Grodzicki, P. Piszczek, A. Bratkowski: *J. Molec. Struct.* **704**(1–3), 107–113 (2004)
- 54.40 A. Boguta, D. Wrobel, A. Bartczak, R. Swietlik, Z. Stachowiak, I. M. Ion: *Mater. Sci. Eng. B Solid* **113**(1), 99–105 (2004)

- 54.41 J. Spadavecchia, G. Ciccarella, S. Capone, R. Rella: *Chem. Mater.* **16**(11), 2083–2090 (2004)
- 54.42 H. Nishimura, M. Iizuka, S. Kuniyoshi, M. Nakamura, K. Kudo, K. Tanaka: *Electron. Commun. Jpn.* **87**(2), 18–25 (2004)
- 54.43 Y. L. Lee, H. Y. Wu, C. H. Chang, Y. M. Yang: *Thin Solid Films* **423**(2), 169–177 (2003)
- 54.44 M. C. Petty: *Langmuir–Blodgett Films: An Introduction* (Cambridge Univ. Press, Cambridge 1996)
- 54.45 M. J. Cook: *J. Mater. Sci. Electron.* **5**, 117–128 (1994)
- 54.46 M. J. Cook: *Int. J. Electron.* **76**, 727–739 (1994)
- 54.47 C. G. Claessens, W. J. Blau, M. Cook, M. Hanack, R. J. M. Nolte, T. Torres, D. Wohrle: *Monatsh. Chem.* **132**(1), 3–11 (2001)
- 54.48 M. J. Cook: *J. Mater. Chem.* **6**, 677–689 (1996)
- 54.49 T. H. Richardson, C. M. Dooling, O. Worsfold, L. T. Jones, K. Kato, K. Shinbo, F. Kaneko, R. Treginning, M. O. Vysotsky, C. A. Hunter: *Colloid Surf. A* **198**, 843–857 (2002)
- 54.50 M. J. Cook, J. McMurdo, D. A. Miles, R. H. Poynter, J. M. Simmons, S. D. Haslam, R. M. Richardson, K. Welford: *J. Mater. Chem.* **4**, 1205–1213 (1994)
- 54.51 A. K. Hassan, A. K. Ray, A. V. Nabok, S. Panigrahi: *IEE Proc. -Sci. Meas. Technol.* **147**, 137–140 (2000)
- 54.52 D. Meyerhofer: *J. Appl. Phys.* **49**, 3993–7 (1978)
- 54.53 P. C. Sukanek: *J. Electrochem. Soc.* **138**, 1712–1719 (1991)
- 54.54 P. C. Sukanek: *J. Electrochem. Soc.* **144**, 3959–3962 (1997)
- 54.55 A. K. Hassan, A. V. Nabok, A. K. Ray, A. Lucke, K. Smith, C. J. M. Stirling, F. Davis: *Supramol. Sci. Mater. Sci. Eng. C* **8–9**, 251–255 (1999)
- 54.56 S. M. Critchley, M. R. Willis, M. J. Cook, J. McMurdo, Y. Maruyama: *J. Mater. Chem.* **2**, 157 (1992)
- 54.57 G. C. Bryant, M. J. Cook, C. Ruggier, T. G. Ryan, A. J. Thorne, S. D. Haslam, R. M. Richardson: *Thin Solid Films* **243**, 316–324 (1994)
- 54.58 X. Li, H. Xu, Q. Zhou, D. Jiang, L. Zhang, A. Lu: *Thin Solid Films* **324**, 277–280 (1998)
- 54.59 K. Bandyopadhyay, S. G. Liu, H. Y. Liu, L. Echegoyen: *Chem. Eur. J.* **6**, 4385–4392 (2000)
- 54.60 C. C. Hsueh, M. T. Lee, M. S. Freund, G. S. Ferguson: *Angew. Chem. Int. Ed.* **39**, 1228–1230 (2000)
- 54.61 H. G. Hong, M. Jiang, S. G. Sligar, P. W. Bohn: *Langmuir* **10**, 153–8 (1994)
- 54.62 K. F. Kelly, Y. B. S. Shon, T. R. Lee, N. J. Halas: *J. Phys. Chem. B* **103**, 8639 (1999)
- 54.63 V. Poderys, A. Selskis, R. Rotomskis: *Solid State Phenom.* **97–98**, 221–224 (2004)
- 54.64 A. Ulman: *An Introduction to Ultrathin Films: From Langmuir–Blodgett to Self-Assembly* (Academic, San Diego 1991)
- 54.65 T. R. E. Simpson, D. A. Russell, I. Chambrier, M. J. Cook, A. B. Horn, S. C. Thorpe: *Sensors Actuat. B* **29**, 353–357 (1995)
- 54.66 M. J. Cook: *Pure Appl. Chem.* **71**(11), 2145–2151 (1999)
- 54.67 K. Ozoemena, P. Westbroek, T. Nyokong: *J. Porphy. Phthalocyan.* **6**(2), 98–106 (2002)
- 54.68 X. Zhang, J. C. Shen: *Adv. Mater.* **11**(13), 1139–1143 (1999)
- 54.69 Y. Lvov, G. Decher, H. Möhwald: *Langmuir* **9**, 481 (1993)
- 54.70 Y. Lvov, K. Ariga, I. Ichinose, T. Kunitake: *J. Am. Chem. Soc.* **117**, 6117 (1995)
- 54.71 Y. M. Lvov, G. Decher: *Crystallogr. Rep.* **39**, 628 (1994)
- 54.72 X. Zhang, M. L. Gao, X. X. Kong, Y. P. Sun, J. C. Shen: *J. Chem. Soc. Chem. Commun.* **9**, 1055–1056 (1994)
- 54.73 C. Q. Sun, X. Y. Zhang, D. Jiang, Q. A. Gao, H. D. Xu, Y. P. Sun, X. Zhang, J. C. Shen: *J. Electroanal. Chem.* **411**(1–2), 73–78 (1996)
- 54.74 D. J. Revell, I. Chambrier, M. J. Cook, D. A. Russell: *J. Mater. Chem.* **10**(1), 31–37 (2000)
- 54.75 M. J. Cook, I. Chambrier: *Phthalocyanine properties*. In: *Porphyrin Handbook*, Vol. 15, ed. by K. Kadish et al. (Academic, New York 2003) Chap. 108
- 54.76 S. Antohe, N. Tomozeiu, S. Gogonea: *Phys. Stat. Sol. (a)* **125**, 397–408 (1991)
- 54.77 M. J. Cook, M. F. Daniel, K. J. Harrison, N. B. Mckewen, A. J. Thomson: *J. Chem. Soc. Chem. Commun.* **15**, 1148–1150 (1987)
- 54.78 M. J. Cook, M. F. Daniel, K. J. Harrison, N. B. Mckewen, A. J. Thomson: *J. Chem. Soc. Chem. Commun.* **14**, 1086–1088 (1987)
- 54.79 A. K. Ray, A. V. Nabok, A. K. Hassan, O. Omar, R. Taylor, M. J. Cook: *Philos. Mag. B* **78**(1), 53–64 (1998)
- 54.80 X. B. Huang, Y. Q. Liu, S. Wang, S. Q. Zhou, D. B. Zhu: *Chem. Eur. J.* **8**(18), 4179–4184 (2002)
- 54.81 C. Granito, L. M. Goldenberg, M. R. Bryce, A. P. Monkman, L. Troisi, L. Pasimeni, M. C. Petty: *Langmuir* **12**(2), 472–476 (1996)
- 54.82 B. N. Achar, P. K. Jayasree: *Can. J. Chem./Rev. Can. Chim.* **77**(10), 1690–1696 (1999)
- 54.83 H. R. Kerp, E. E. van Faassen: *Proceedings of the 11th Workshop on Quantum Solar Energy Conversion – (QUANTSOL'98)*, *Chem. Phys. Lett.* **332**, 5 (2000)
- 54.84 P. D. Hooper, M. I. Newton, G. McHaleand, M. R. Willis: *Semicond. Sci. Technol.* **12**, 455–459 (1997)
- 54.85 D. Markovitsi, T. H. Tran-Thi, R. Even, J. Simon: *Chem. Phys. Lett.* **137**, 107 (1987)
- 54.86 T. Basova, E. Kol'tsov, A. K. Hassan, A. Nabok, A. G. Gurek, V. Ahsen: *J. Mater. Sci.–Mater. El.* **15**(9), 623–628 (2004)
- 54.87 W. Snow, W. R. Barger: *Phthalocyanine films in chemical sensors*. In: *Phthalocyanines. Properties and Applications*, ed. by C. C. Leznoff, A. B. P. Lever (VCH, New York 1989)
- 54.88 M. Nicolau, B. del Rey, T. Torres, C. Mingotaud, P. Delhaes, M. J. Cook, S. C. Thorpe: *Synth. Met.* **102**(1–3), 1462–1463 (1999)
- 54.89 R. Zhou, F. Josse, W. Gopel, Z. Z. Öztürk, Ö. Bekaroglu: *Appl. Organomet. Chem.* **10**, 557–577 (1996)

- 54.90 A. Chyla, A. Lewandowska, J. Soloducho, A. Gorecka-Drzazga, M. Szablewski: *IEEE Trans. Dielect. El In* **8**(3), 559–565 (2001)
- 54.91 S. Gao, H. Zhao, L. H. Huo, J. G. Zhao, Y. Q. Wu, S. Q. Xi: *Sensors Actuat. B Chem.* **97**(2–3), 319–323 (2004)
- 54.92 S. Suslick, N. A. Rakow, M. E. Kosal, J.–H. Chou: *J. Porphy. Phthalocyan.* **4**, 407–413 (2001)
- 54.93 Y. Lee, B. K. Oh, M. E. Meyerhoff: *Anal. Chem.* **76**(3), 536–544 (2004)
- 54.94 J. Charvatova, O. Rusin, V. Kral, K. Volka, P. Matejka: *Sensors Actuat. B* **76**(1–3), 366–372 (2001)
- 54.95 O. Ikeda, H. Koyama, K. Kijima, T. Komura, A. Itajima, M. Miyake, K. Yamamoto, A. Yamatodani: *Proceedings of the 27th Chemical Sensor Symposium*, Vol. 14 (Supplement B) (Japan Association of Chemical Sensor, Nagaoka University of Technology October 23–24, 1998) pp. 89–92
- 54.96 V. C. Smith, T. Richardson, H. L. Anderson: *Supramolec. Sci.* **4**(3–4), 503–508 (1997)
- 54.97 V. Arima, R. I. R. Blyth, F. Della Sala, R. Del Sole, F. Matino, G. Mele, G. Vasapollo, R. Cingolani: *Mater. Sci. Eng. C Bio. Solids* **24**(4), 569–573 (2004)
- 54.98 H. Imahori, K. Hosomizu, Y. Mori, T. Sato, T. K. Ahn, S. K. Kim, D. Kim, Y. Nishimura, I. Yamazaki, H. Ishii, H. Hotta, Y. Matano: *J. Phys. Chem. B* **108**(16), 5018–5025 (2004)
- 54.99 Q. L. Li, S. Surthi, G. Mathur, S. Gowda, Q. Zhao, T. A. Sorenson, R. C. Tenent, K. Muthukumar, J. S. Lindsey, V. Misra: *Appl. Phys. Lett.* **85**(10), 1829–1831 (2004)
- 54.100 K. E. Splan, J. T. Hupp: *Langmuir* **20**(24), 10560–10566 (2004)
- 54.101 J. R. C. da Rocha, G. J. F. Demets, M. Bertotti, K. Araki, H. E. Toma: *J. Electroanal. Chem.* **526**(1–2), 69–76 (2002)
- 54.102 J. D. Wright: *Prog. Surf. Sci.* **31**(1–2), 1–60 (1989)
- 54.103 J. P. Germain, A. Pauly, C. Maleysson, J. P. Blanc, B. Schöllhorn: *Thin Solid Films* **333**, 235–239 (1998)
- 54.104 B. Schöllhorn, J. P. Germain, A. Pauly, C. Maleysson, J. P. Blanc: *Thin Solid Films* **326**, 245–250 (1998)
- 54.105 J. Travis, A. K. Ray, S. C. Thorpe, M. J. Cook, S. A. James: *Meas. Sci. Technol.* **6**(7), 988–994 (1995)
- 54.106 A. Cole, R. J. McIlroy, S. C. Thorpe, M. J. Cook, J. McMurdo, A. K. Ray: *Sensors Actuat. B* **13**, 416–419 (1993)
- 54.107 D. Crouch, S. C. Thorpe, M. J. Cook, I. Chambrier, A. K. Ray: *Sensors Actuat. B* **18–19**, 411–414 (1994)
- 54.108 A. Tepore, A. Serra, D. P. Arnold, D. Manno, G. Micocci, A. Genga, L. Valli: *Langmuir* **17**(26), 8139–8144 (2001)
- 54.109 Y. L. Lee, C. Y. Sheu, R. H. Hsiao: *Sensors Actuat. B Chem.* **99**(2–3), 281–287 (2004)
- 54.110 Y. L. Lee, C. H. Hsiao, C. H. Chang, Y. M. Yang: *Sens. Actuat. B* **94**, 169–175 (2003)
- 54.111 M. I. Newton, T. K. H. Starke, G. McHale, M. R. Willis: *Thin Solid Films* **360**(1–2), 10–12 (2000)
- 54.112 M. I. Newton, T. K. H. Starke, M. R. Willis, G. McHale: *Sens. Actuat. B* **67**, 307–311 (2000)
- 54.113 Q. Zhou, R. D. Gould: *Thin Solid Films* **317**(1–2), 436–439 (1998)
- 54.114 W. F. Qiu, W. P. Hu, Y. Q. Liu, S. Q. Zhou, Y. Xu, D. B. Zhu: *Sensors Actuat. B Chem.* **75**(1–2), 62–66 (2001)
- 54.115 M. Bouvet, A. Leroy, J. Simon, F. Tournilhac, G. Guillaud, P. Lessnick, A. Maillard, S. Spirkovitch, M. Debligny, A. Haan, A. Decroly: *Sensors Actuat. B Chem.* **72**(1), 86–93 (2001)
- 54.116 M. Bouvet, G. Guillaud, A. Leroy, A. Maillard, S. Spirkovitch, F. G. Tournilhac: *Sensors Actuat. B Chem.* **73**(1), 63–70 (2001)
- 54.117 C. Q. Sun, Y. P. Sun, X. Zhang, H. D. Xu, J. C. K. Shen: *Anal. Chim. Acta* **312**(2), 207–212 (1995)
- 54.118 Y. P. Sun, X. Zhang, C. Q. Sun, Z. Q. Wang, J. C. Shen, D. J. Wang, T. J. Li: *Chem. Commun.* **20**, 2379–2380 (1996)
- 54.119 K. F. Schoch, J. Gregg, T. A. Temofonte: *J. Vac. Sci. Technol. A* **6**(1), 155–158 (1988)
- 54.120 A. K. Hassan, A. K. Ray, J. R. Travis, Z. Ghassemlooy, M. J. Cook, A. Abass, R. A. Collins: *Sensors Actuat. B Chem.* **49**(3), 235–239 (1998)
- 54.121 J. Mårtensson, H. Arwin, I. Lundstrom: *Sensors Actuat. B Chem.* **1**(1–6), 134–137 (1990)
- 54.122 J. M. Pedrosa, C. M. Dooling, T. H. Richardson, R. K. Hyde, C. A. Hunter, M. T. Martin, L. Camacho: *J. Mater. Chem.* **12**(9), 2659–2664 (2002)
- 54.123 O. Worsfold, C. M. Dooling, T. H. Richardson, M. O. Vysotsky, R. Tregonning, C. A. Hunter, C. Mallins: *Colloid Surf. A* **198**, 859–867 (2002)
- 54.124 L. Gaffo, O. D. D. Couto, R. Giro, M. J. S. P. Brasil, D. S. Galvao, F. Cerdeira, O. N. de Oliveira, K. Wohnrath: *Solid State Commun.* **131**(1), 53–56 (2004)
- 54.125 T. Richardson, V. C. Smith, A. Topaçli, J. Jiang, C. H. Huang: *Supramol. Sci.* **4**, 465–470 (1997)
- 54.126 T. R. E. Simpson, M. J. Cook, M. C. Petty, S. C. Thorpe, D. A. Russell: *Analyst* **121**(10), 1501–1505 (1996)
- 54.127 T. R. E. Simpson, D. J. Revell, M. J. Cook, D. A. Russell: *Langmuir* **13**(3), 460–464 (1997)
- 54.128 E. Kretschmann: *Z. Phys.* **241**, 313–324 (1971)
- 54.129 I. Pockrand: *Surf. Sci.* **72**, 577–588 (1978)
- 54.130 J. M. Rooney, E. A. H. Hall: *Anal. Chem.* **76**(23), 6861–6870 (2004)
- 54.131 T. Basova, E. Kol'tsov, A. Hassan, A. Tsgorodskaya, A. K. Ray, I. Igumenov: *Phys. Stat. Sol. (b)* **242**(4), 822 (2005)
- 54.132 J. D. Wright, A. Cado, S. J. Peacock, V. Rivalle, A. M. Smith: *Sens. Actuat. B* **29**, 108–114 (1995)
- 54.133 J. P. Lloyd, C. Pearson, M. C. Petty: *Thin Solid Films* **160**(1–2), 431–443 (1988)
- 54.134 M. J. Jory, P. S. Cann, J. R. Sambles: *J. Phys. D Appl. Phys.* **27**(1), 169–174 (1994)
- 54.135 K. Kato, C. M. Dooling, K. Shinbo, T. H. Richardson, F. Kaneko, R. Tregonning, M. O. Vysotsky, C. A. Hunter: *Colloid Surf. A* **198**, 811–816 (2002)

- 54.136 D. S. Ballantine, R. M. White, S. I. Martin, A. J. Ricco, E. T. Zellers, G. C. Fry, H. Wohltjen: *Acoustic Wave Sensors. Theory, Design, and Physico-Chemical Applications* (Academic, New York 1997)
- 54.137 K. D. Schierbaum, R. Zhou, S. Knecht, R. Dieing, M. Hanack, W. Göpel: *Sensors Actuat. B Chem.* **24**, 69–71 (1995)
- 54.138 H. Ding, V. Erokhin, M. K. Ram, S. Paddeu, L. Valkova, C. Nikolini: *Thin Solid Films* **379**, 279–286 (2000)
- 54.139 Z. Z. Öztürk, R. Zhou, U. Weimar, V. Ahsen, O. Bekaroğlu, W. Göpel: *Sensors Actuat. B Chem.* **26–27**, 208–212 (1995)
- 54.140 J. Souto, M. L. Rodriguez, J. A. Desaja, R. Aroca: *Int. J. Electron.* **76**(5), 763–769 (1994)
- 54.141 T. Basova, C. Tasaltin, A. G. Gurek, M. A. Ebeoğlu, Z. Z. Öztürk, V. Ahsen: *Sensors Actuat. B Chem.* **96**(1–2), 70–75 (2003)
- 54.142 C. Barriain, I. R. Matias, C. Fernandez-Valdivielso, F. J. Arregui, M. L. Rodriguez-Mendez, J. A. de Saja: *Sensors Actuat. B Chem.* **93**(1–3), 153–158 (2003)
- 54.143 J. Spadavecchia, G. Ciccarella, R. Rella, S. Capone, P. Siciliano: *Sensors Actuat. B Chem.* **96**(3), 489–497 (2003)
- 54.144 J. Spadavecchia, G. Ciccarella, A. Buccolieri, G. Vasapollo, R. Rella: *J. Porphy. Phthalocyan.* **7**(8), 572–578 (2003)
- 54.145 S. Nardis, D. Monti, C. Di Natale, A. D'Amico, P. Siciliano, A. Forleo, M. Epifani, A. Taurino, R. Rella, R. Paollesse: *Sensors Actuat. B Chem.* **103**(1–2), 339–343 (2004)
- 54.146 J. Spadavecchia, G. Ciccarella, G. Vasapollo, P. Siciliano, R. Rella: *Sensors Actuat. B Chem.* **100**(1–2), 135–138 (2004)
- 54.147 C. Granito, J. N. Wilde, S. Houghton, P. J. Iredale: *Thin Solid Films* **284–285**, 98–101 (1996)
- 54.148 G. Jin, C. O. Too, J. Norrish, G. G. Wallace: *Synth. Met.* **135**(1–3), 29–30 (2003)
- 54.149 V. Papes, S. Brodska: *Sensors Actuat. B Chem.* **40**, 143–145 (1997)
- 54.150 A. Riul, A. M. G. Soto, S. V. Mello, S. Bone, D. M. Taylor, L. H. C. Mattoso: *Synth. Met.* **132**(2), 109–116 (2003)
- 54.151 J. S. Do, W. B. Chang: *Sensors Actuat. B Chem.* **101**(1–2), 97–106 (2004)
- 54.152 G. Anitha, E. Subramanian: *Sensors Actuat. B Chem.* **92**(1–2), 49–59 (2003)
- 54.153 E. Segal, R. Tchoudakov, M. Narkis, A. Siegmann, Y. Wei: *Sensors Actuat. B Chem.* **104**(1), 140–150 (2005)
- 54.154 E. Milella, F. Musio, M. B. Alba: *Thin Solid Films* **285**, 908 (1996)
- 54.155 Y. Kunugi, K. Nigorikawa, Y. Harima, K. Yamashita: *J. Chem. Soc. Chem. Commun.* **Issue 7**, 873 (1994)
- 54.156 S. Christie, E. Scorsone, K. Persaud, F. Kvasnik: *Sensors Actuat. B Chem.* **90**(1–3), 163–169 (2003)
- 54.157 M. Ando, C. Swart, E. Pringsheim, V. M. Mirsky, O. S. Wolfbeis: *Solid State Ionics* **152–153**, 819–822 (2002)
- 54.158 A. Penza, G. Cassano, A. Sergi, C. Lo Sterzo, M. Russo: *Sensors Actuat. B Chem.* **81**(1), 88–98 (2001)
- 54.159 T. A. Dickinson, J. White, J. S. Kauer, D. R. Walt: *Nature* **382**, 697 (1996)
- 54.160 D. Li, C. A. Mills, J. M. Cooper: *Sensors Actuat. B Chem.* **92**(1–2), 73–80 (2003)
- 54.161 T. Jeong, H. K. Lee, D. C. Jeong, S. Jeon: *Talanta* **65**(2), 543–548 (2005)
- 54.162 M. M. Ardakany, A. A. Ensafi, H. Naeimi, A. Dastanpour, A. Shamli: *Sensors Actuat. B Chem.* **96**(1–2), 441–445 (2003)
- 54.163 S. Y. Huan, C. X. Jiao, Q. Shen, J. H. Jiang, G. M. Zeng, H. H. Guo, S. L. Guo, R. Q. Yu: *Electrochim. Acta* **49**(25), 4273–4280 (2004)
- 54.164 P. A. Antunes, C. M. Santana, R. F. Aroca, O. N. Oliveira, C. J. L. Constantino, A. Riul: *Synth. Met.* **148**(1), 21–24 (2005)
- 54.165 T. Shimanouchi, S. Morita, H. S. Jung, Y. Sakurai, Y. Suzuki, R. Kuboi: *Sensor Mater.* **16**(5), 255–265 (2004)
- 54.166 P. C. Ewbank, R. S. Loewe, L. Zhai, J. Reddinger, G. Sauve, R. D. McCullough: *Tetrahedron* **60**(49), 11269–11275 (2004)
- 54.167 J. N. Wilde, J. Nagel, M. C. Petty: *Thin Solid Films* **327–329**, 726–729 (1998)
- 54.168 R. Casalini, J. N. Wilde, J. Nagel, U. Oertel, M. C. Petty: *Sensors Actuat. B* **57**, 28–34 (1999)
- 54.169 J. K. Abraham, B. Philip, A. Witchurch, V. K. Varadan, C. C. Reddy: *Smart Mater. Struct.* **13**(5), 1045–1049 (2004)
- 54.170 B. Philip, J. K. Abraham, A. Chandrasekhar, V. K. Varadan: *Smart Mater. Struct.* **12**(6), 935–939 (2003)
- 54.171 R. Capan, A. K. Ray, A. K. Hassan, T. Tanrisever: *J. Phys. D Appl. Phys.* **36**, 1115–1119 (2003)
- 54.172 R. Rego, N. Caetanoc, R. Vale, A. Mendes: *J. Membr. Sci.* **244**(1–2), 35–44 (2004)
- 54.173 M. Matsuguchi, A. Okamoto, Y. Sakai: *Sensors Actuat. B Chem.* **94**(1), 46–52 (2003)
- 54.174 J. Sutter, A. Radu, S. Peper, E. Bakker, E. Pretsch: *Anal. Chim. Acta* **523**(1), 53–59 (2004)
- 54.175 C. Ramesh, G. Velayutham, N. Murugesan, V. Ganeshan, V. Manivannan, G. Periaswami: *Ionics* **10**(1–2), 50–55 (2004)
- 54.176 A. Calogirou, M. Duan, D. Kotzias, M. Lahaniati, B. R. Larsen: *Atmos. Environ.* **31**, 2741 (1997)
- 54.177 A. V. Nabok, A. K. Hassan, A. K. Ray, J. Travis, M. Hofton, A. Dalley: *IEE Proc. Sci., Meas. Technol.* **147**, 153 (2000)
- 54.178 A. K. Ray, A. V. Nabok, A. K. Hassan, M. Hofton, A. Dalley: *Sensors & Their Applications X Conference*, ed. by N. M. White, J. T. Augousti (1999)

- 54.179 A. K. Hassan, A. V. Nabok, A. K. Ray, G. Kiousis: Mater. Sci. Eng. C **22**, 197–200 (2002)
- 54.180 A. K. Hassan, J. Greenway, A. K. Ray, A. V. Nabok: J. Phys. D Appl. Phys. **36**(17), 2130–2133 (2003)
- 54.181 B. Ding, J. H. Kim, Y. Miyazaki, S. M. Shiratori: Sensors Actuat. B Chem. **101**(3), 373–380 (2004)
- 54.182 Z. Cao, D. Cao, Z. G. Lei, H. G. Lin, R. Q. Yu: Talanta **44**, 1413 (1997)
- 54.183 C. D. Gutsche: *Calixarenes* (Royal Society of Chemistry, Cambridge 1989)
- 54.184 D. J. Cram, S. Karbach, H.-E. Kim, C. B. Knober, E. F. Maverick, J. L. Ericson, R. C. Hegelson: J. Am. Chem. Soc. **110**, 2229 (1988)
- 54.185 F. L. Dickert, U. P. A. Baumler, G. K. Zwissler: Synth. Met. **61**, 47 (1993)
- 54.186 P. Nelli, E. Delcanale, G. Faglia, G. Sberveglieri, P. Soncini: Sensors Actuat. B Chem. **13–14**, 302 (1993)
- 54.187 T. Weiss, K. D. Schierbaum, W. Göpel, U. Thoden van Velzen, D. N. Reinhoudt: Sensors Actuat. B Chem. **26**, 203 (1995)
- 54.188 E. Dalcanale, J. Hartman: Sensors Actuat. B Chem. **24**, 39 (1995)
- 54.189 J. Rickert, T. Weiss, W. Gopel: Sensors Actuat. B Chem. **31**, 45 (1996)
- 54.190 A. K. Hassan, A. K. Ray, A. V. Nabok, F. Davis: Sensors Actuat. B **77**, 638–641 (2001)
- 54.191 A. V. Nabok, N. V. Lavrik, Z. I. Kazantseva, B. A. Nesterenko, L. N. Markovskiy, V. I. Kalchenko, A. V. Shivaniuk: Thin Solid Films **259**, 244–247 (1995)
- 54.192 A. V. Nabok, A. K. Hassan, A. K. Ray: J. Mater. Chem. **10**, 189–194 (2000)
- 54.193 A. V. Nabok, A. K. Hassan, A. K. Ray, O. Omar, V. I. Kalchenko: Sensors Actuat. B Chem. **45**, 115 (1997)
- 54.194 A. K. Hassan, A. K. Ray, A. V. Nabok, T. Willkop: Appl. Surf. Sci. **182**, 49–54 (2001)
- 54.195 S. J. Gregg, K. S. W. Sing: *Adsorption, Surface Area and Porosity* (Academic, New York 1967)
- 54.196 T. Willkop, A. K. Ray: J. Phys. D Appl. Phys. **35**(20), 2661–2667 (2002)
- 54.197 P. Gouma, G. Sberveglieri, R. Dutta, J. W. Gardner, E. L. Hines: MRS Bull. **29**(10), 697–700 (2004)
- 54.198 A. V. Shevade, M. A. Ryan, M. L. Homer, A. M. Manfreda, H. Zhou, K. S. Manatt: Sensors Actuat. B Chem **93**(1–3), 84–91 (2003)
- 54.199 A. Mills, S. L. Hunte: J. Photochem. Photobiol. A **108**, 1–35 (1997)
- 54.200 G. J. Wilson, G. D. Will: Curr. Appl. Phys. **4** (2–4), 351–354 (2004)
- 54.201 D. Chatterjee, A. Mahata: J. Photochem. Photobiol. **153**(1–3), 199–204 (2002)
- 54.202 L. R. Skubal, N. K. Meshkov, M. C. Vogt: J. Phototechnol. Photobiol. A **148**(1–3), 103–108 (2002)